

The ROSAT All-Sky Survey: a Catalog of Clusters of Galaxies in a Region of 1 Ster around the South Galactic Pole

R. Cruddace^{1,2}, W. Voges³, H. Böhringer³, C. A. Collins⁴, A. K. Romer⁵, H. MacGillivray⁶,
D. Yentis¹, P. Schuecker³, H. Ebeling⁷, and S. De Grandi⁸

ABSTRACT

A field of 1.013 ster in the ROSAT all-sky survey (RASS), centered on the south galactic pole (SGP), has been searched in a systematic, objective manner for clusters of galaxies. The procedure relied on a correlation of the X-ray positions and properties of ROSAT sources in the field with the distribution of galaxies in the COSMOS digitised data base, which was obtained from scanning the plates of the UK Schmidt IIIa-J optical survey of the southern sky. The study used the second ROSAT survey data base (RASS-2) and included several optical observing campaigns to measure cluster redshifts. The search, which is a precursor to the larger REFLEX survey encompassing the whole southern sky, reached the detection limits of both the RASS and the COSMOS data, and yielded a catalog of 186 clusters in which the lowest flux is 1.5×10^{-12} erg cm⁻² s⁻¹ in the 0.1 – 2.4 keV band. Of these 157 have measured redshifts. Using a flux limit of 3.0×10^{-12} erg cm⁻² s⁻¹ a complete subset of 112 clusters was obtained, of which 110 have measured redshifts. The spatial distribution of the X-ray clusters out to a redshift of 0.15 shows an extension of the Local Supercluster to the Pisces-Cetus supercluster ($z < \sim 0.07$), and an orthogonal structure at higher redshift ($0.07 < z < 0.15$). This result is consistent with large-scale structure suggested by optical surveys.

¹E. O. Hulburt Center for Space Research, Naval Research Laboratory, Washington DC 20375

²Visiting Scientist, Max-Planck-Institut für Extraterrestrische Physik, 85740 Garching, Germany

³Max-Planck-Institut für Extraterrestrische Physik, 85740 Garching, Germany

⁴Astrophysics Research Institute, Liverpool John Moores University, Liverpool L3 5AF, England

⁵Carnegie Mellon University, 5000 Forbes Avenue, Pittsburgh, Pennsylvania 15213

⁶Institute of Astronomy, University of Edinburgh, Blackford Hill, Edinburgh EH9 3HJ, Scotland

⁷Institute for Astronomy, University of Hawaii, 2680 Woodlawn Drive, Honolulu, Hawaii 96822

⁸Osservatorio Astronomico di Brera, via Bianchi 46, 22055 Merate (LC), Italy

INTRODUCTION

It has been recognized for many years that observations of clusters of galaxies can be applied effectively to test theories of the evolution of the universe. As the largest gravitationally bound objects emerging from the growth and subsequent collapse of primordial density fluctuations, their spatial distribution at different epochs is a relic containing evidence which can test cosmological models of structure formation. X-ray astronomy has enhanced the results of such studies greatly, for a number of reasons. First, clusters are X-ray sources of relatively high luminosity, with a luminosity function sufficiently well defined to allow, in principle at least, cosmic structure to be studied out to epochs of $z \sim 1$ and beyond. Further, ambiguities in the identification of clusters, caused by chance line-of-sight superposition of objects, are fewer in X-ray than in optical sky surveys. This is a consequence of the sharply peaked X-ray brightness distribution in most clusters, and of the relatively low surface density of bright X-ray sources. Second, the X-ray properties of clusters are defined by events reaching back to the earliest epoch of cluster formation, and therefore may be used to test cosmological models. The X-ray luminosity and temperature of the intracluster gas depend on the cluster mass, so that the shape and amplitude of the luminosity and temperature functions of the cluster population are dependent on the spectrum of the early density perturbations. Further, the morphology of clusters in the whole population may be dependent on the characteristics of the expansion, and is a diagnostic of cluster merging processes. Finally, the abundance of heavy elements in the intracluster gas is a measure of galaxy evolution and ram-pressure stripping, and of the proportion of primordial gas in the cluster.

Therefore much effort has been given to the production of statistically complete samples of X-ray emitting clusters. The first were produced using *Uhuru* (Schwartz 1978) and *Ariel V* (McHardy 1978) observations, and the HEAO-1 all-sky surveys (Piccinotti et al. 1982; Kowalski et al. 1984), and contained up to 76 clusters. The flux limits of these surveys ($1-8 \times 10^{-11}$ erg cm $^{-2}$ s $^{-1}$, expressed here in the ROSAT band 0.1–2.4 keV), and their angular resolution were limited by the use of proportional counters, and improvements were possible only after the first missions using imaging X-ray instruments. Edge et al. (1990) reported the use of EINSTEIN and EXOSAT observations to refine the results of the earlier surveys, producing a sample of 55 clusters free of, for example, the effects of source confusion. In the EINSTEIN Extended Medium Sensitivity Survey (EMSS) it was possible, by examining the fields of EINSTEIN pointings covering a total of 740 deg 2 , to create a sample with a flux limit of 1.3×10^{-13} erg cm $^{-2}$ s $^{-1}$ (0.3 – 3.5 keV) and containing clusters with redshifts out to $z = 0.58$ (Henry et al. 1992).

The ROSAT X-ray telescope, equipped with an imaging proportional counter in the focal

plane, allowed for the first time complete detailed surveys of large areas of sky (Trümper 1983). The analysis of the ROSAT All-Sky Survey (RASS) proceeded in two phases RASS-1 and RASS-2, described below in section 3.1, in which the second phase incorporated a number of improvements suggested by RASS-1 (Voges et al. 1999). The first X-ray flux-limited samples of clusters based on analysis of a large area of sky in the ROSAT survey were obtained by Romer et al.(1994), Romer (1995), Ebeling et al.(1996) and Ebeling et al. (1998). The SGP sample described in Romer et al.(1994), based on analysis of the RASS-1 data base, contained 161 cluster candidates with a limiting flux of 10^{-12} erg cm $^{-2}$ s $^{-1}$ (0.1 – 2.4 keV). Redshifts were obtained for 128 clusters in this sample, and this subset was used in a study of the cluster spatial correlation function (Romer et al. 1994). The BCS survey by Ebeling et al. (1998) addressed the whole extragalactic sky ($b \geq 20^\circ$) in the northern hemisphere, and reanalysed the fields in which clusters had been detected in the RASS-1 analysis. The survey yielded a sample of 201 clusters at $z \leq 0.3$, having a limiting flux of 4.4×10^{-12} erg cm $^{-2}$ s $^{-1}$ (0.1 – 2.4 keV), which is statistically complete at the 90 percent level. In a recent publication the BCS sample has been extended to an X-ray flux limit of 2.8×10^{-12} erg cm $^{-2}$ s $^{-1}$, at which the completeness was 75 percent (Ebeling et al. 2000). A recent survey of clusters in the northern sky (NORAS), based on X-ray sources classified as extended in the RASS analysis, is described by Böhringer et al. (2000). Deeper surveys have been possible in areas around the ecliptic poles (Henry et al. 2001, Gioia et al. 2001, Mullis et al. 2001 and Voges et al. 2001), where the ROSAT survey achieved unusually long exposure times, and in areas where deep pointings have been made (Romer et al. 2000, Jones et al. 1998, Rosati et al. 1998, Vikhlinen et al. 1998 and Collins et al. 1997). The deepest survey was made by Rosati et al. (1998), in which the sample was complete down to a flux of 4×10^{-14} erg cm $^{-2}$ s $^{-1}$ and included clusters out a redshift of $z \sim 0.8$.

In what follows we concentrate on complete large-area cluster surveys in the southern hemisphere. This has its roots in an agreement between the Royal Observatory in Edinburgh (ROE), the Naval Research Laboratory (NRL) and the Max-Planck-Institut für Extraterrestrische Physik (MPE) in Garching, made early in the ROSAT program, to make the COSMOS digitised UK Schmidt IIIa-J survey of the southern sky (MacGillivray & Stobie 1985, Yentis et al. 1992) available for identification of X-ray sources. This data base, containing 3.5×10^8 objects with a limiting magnitude of $b_j \sim 22$, was installed at MPE for use in X-ray source identification. In cluster studies it was used to derive unbiased lists of candidates through systematic correlations of X-ray source positions with concentrations of galaxies. A comprehensive search for clusters is being undertaken at MPE in the REFLEX southern hemisphere project (Böhringer et al. 2001). The first results (De Grandi et al. 1999) described a sample of X-ray bright clusters, obtained by searching a region of area 8235 deg 2 (2.5 ster). The study reanalysed clusters identified in the RASS-1 analysis and

arrived at a sample of 130 clusters having a completeness of at least 90 percent and a limiting flux of $5 - 6.6 \times 10^{-12} \text{ erg cm}^{-2} \text{ s}^{-1}$ in the 0.1 – 2.4 keV band. The complete REFLEX study area covers 4.24 ster in the southern sky, and the techniques used in constructing the cluster sample have been described by Böhringer et al. (2001). At the current stage of the study a sample of 452 clusters has been obtained, which is at least 90 percent complete, using a flux limit of $3 \times 10^{-12} \text{ erg cm}^{-2} \text{ s}^{-1}$. A power-law fit to the log N-log S distribution yielded an exponent of $\alpha = -1.39 \pm 0.07$. Collins et al. (2000) have analysed the spatial correlation function of clusters using a REFLEX sample of 452 clusters covering an area 4 times larger than the SGP, and derived a value of $18.8 \pm 0.9 \text{ h}^{-1} \text{ Mpc}$ for the correlation length, significantly greater than the value of $12.9 \pm 2.2 \text{ h}^{-1} \text{ Mpc}$ obtained by Romer et al. (1994). However for the 109 REFLEX clusters in the SGP area Collins et al. (2000) find a correlation length of $12.9 \pm 1.9 \text{ h}^{-1} \text{ Mpc}$, consistent with the result of Romer et al. (1994). The difference between the complete REFLEX and the SGP results is most likely due to sample fluctuations caused by cosmic variance (see Collins et al. 2000). A significant conclusion of the REFLEX study is that low-density cold dark matter (CDM) models ($\Omega \sim 0.3$) provide a better fit to the observed correlation function, and that high-density CDM models ($\Omega \sim 1$) yield a poorer fit because they provide insufficient power at large scales. Schuecker et al. (2001) have analysed the power spectrum of the REFLEX sample, and the results are consistent with the results of Collins et al. (2000).

A prominent aspect of the SGP and REFLEX survey projects has been optical observing programs to obtain cluster redshifts, which we describe briefly in section 2. However, it should be borne in mind that while these two projects have a common root and have followed similar procedures for cluster selection, X-ray analysis and redshift determination, they do possess some differences in approach.

Following this introduction section 2 provides a summary of how the SGP survey was performed. Section 3 describes the various procedures by which the cluster sample was extracted from the RASS-2 data base and section 4 summarises how the X-ray energy flux and luminosity were calculated. Section 5 presents the SGP cluster catalog in the form of a table and describes the archive of SGP cluster images in the form of overlays of the X-ray and optical data, which is accessible at MPE over the Internet. Section 6 examines the completeness of the cluster sample and section 7 discusses the large-scale structure traced by the clusters out to a redshift of $z \sim 0.15$. Finally a summary of the results and conclusions of the paper are presented in section 8. Throughout the article we have assumed that the Hubble constant $H_0 = 50 \text{ km s}^{-1} \text{ Mpc}^{-1}$, the deceleration parameter $q_0 = 0.5$ and the cosmological constant $\Lambda = 0$.

2. SUMMARY OF THE SOUTH GALACTIC POLE SURVEY

This survey selected a region at high galactic latitude in the southern sky centered on the South Galactic Pole. Rectangular in shape, it extends in right ascension from 22^{h} to $3^{\text{h}} 20^{\text{m}}$ and in declination from -50° to $+2.5^{\circ}$ (see Figure 17), giving it an area of 1.013 steradian. The search for clusters in this region invoked no flux threshold, but instead worked to the limit of the RASS data to maximise the completeness of the sample of cluster candidates. A flux limit is established subsequently to define a complete subsample.

The first step in the search for clusters was to select all X-ray sources found in the region by the RASS-2 analysis (Voges et al. 1999). In this analysis the threshold values for the source detection algorithms were lowered (section 3.1), with the aim of achieving as deep a survey as the RASS would allow. Therefore cluster searches using this data base have more sensitivity than has been available to previous southern hemisphere searches using the RASS-1 data base (Romer 1995, De Grandi et al. 1999).

The RASS-2 analysis was not equipped for detailed examination of the X-ray properties of extended sources such as clusters. To this end a number of techniques have been developed, including Voronoi Tessellation and Percolation (VTP, Ebeling & Wiedemann 1993), the Steepness Ratio Technique (SRT, DeGrandi et al. 1997) and the Growth Curve Analysis (GCA, Böhringer et al. 2000). The goal of these techniques is to obtain reliable fluxes for both extended and point sources, and to extract from the raw data as much information as possible about the X-ray source characteristics. In this study the GCA technique has been used to analyse the list of candidates obtained from the RASS-2 data base.

Cluster candidates were selected from this sample using the COSMOS digitised IIIa-J survey and a search procedure called CSEARCH. This procedure, which is not designed to select clusters in an unambiguous manner, compares the galaxy density around the RASS-2 position with the background galaxy density on the UK Schmidt plate, and derives a probability that the result was a random coincidence. A sample of cluster candidates is obtained by setting a threshold to this probability, and this threshold is set low enough to ensure that few genuine clusters are lost and a high completeness is attained in the final sample. In our study a RASS-2 list of 11981 sources is reduced by CSEARCH to 3236 candidates (section 3.3). At this point much remains to be done to remove contaminating sources, which we estimate from internal statistical tests to comprise about half the candidates, in an objective process. At high redshifts ($z > \sim 0.3$) the method reaches a limit of the COSMOS data, when many cluster galaxies become so faint as to be classified by COSMOS only as 'faint objects', which are not counted by CSEARCH. Therefore some clusters at high redshift may be missed, which may be one source of incompleteness near the flux limit of the survey.

The analysis of this sample of cluster candidates began by setting a limit of 0.08 ct s^{-1} to the X-ray count rate in the hard band ($0.5 - 2.0 \text{ keV}$, section 3.1, 3.4), which reduced the number of candidates from 3236 to 477. This was followed by the process of removing contaminating sources from this sub-sample, which proceeded through a number of stages. The first was the removal of COSMOS artifacts, bright sources which to the eye were clearly not clusters, and redundant detections by RASS-2 of the same source, particularly in extended sources such as clusters. This was done by examination of COSMOS optical finding charts and of overlays of the optical and X-ray images. The second was to correlate RASS-2 positions with the SIMBAD catalog, in order to eliminate bright stars found in the RASS-2 error circle, and then to use two X-ray properties of the source, hardness ratio and extent, as selection criteria. The hardness ratio was used to exclude those stars and active galactic nuclei (AGN) whose spectra are sufficiently soft to exclude the possibility that the source is a cluster. The X-ray extent was used to classify candidates in three groups, namely clusters, AGN candidates and a remainder of uncertain nature. The third and final stage, identifying the clusters and known AGN among the remaining sample, proceeded along two parallel paths. The first comprised correlations of the candidate list with a variety of catalogs, in particular the NASA Extragalactic Data base (NED), the SIMBAD catalog, and the Veron catalog of AGN (Veron-Cetty & Veron 1998). The second was an ongoing examination of the results of the supporting optical observations, described below, which identified AGN in the sample.

We summarise here briefly the sources of incompleteness in the final catalog obtained, which reduce the cluster count at low fluxes:

- i) The CSEARCH analysis has a predetermined level of incompleteness in correlating X-ray sources with galaxy concentrations (section 3.3).
- ii) The sharp count-rate limit (0.08 ct s^{-1}) rejects some sources at low energy flux, due to the variation of interstellar column density in the field (section 3.4).
- iii) Some distant clusters elude the tests applied in searching the list of candidates yielded by CSEARCH and the X-ray count-rate cut (Section 3.5).

Finally, a vital complementary part of the SGP survey and the REFLEX project has been a program of optical observations to obtain the redshifts of those clusters detected in the ROSAT survey, for which no redshifts were available in the literature. The SGP survey, which commenced not long after the launch of ROSAT in 1990, was supported by three campaigns at the 4m Anglo-Australian Telescope (AAT) and three at the 1.9m telescope of the South African Astronomical Observatory. The results of these campaigns have been reported by Romer (1995). A larger program, which started in 1992 and was completed in 1995, was installed as a Key Project at the European Southern Observatory (ESO). Its

purpose was to obtain redshifts for clusters in the REFLEX sample. An ongoing continuation of these observations is being pursued to support the extension of the REFLEX survey to lower X-ray flux limits.

3. SELECTION OF THE CLUSTER SAMPLE.

3.1 The X-ray Data Base.

The ROSAT observatory was launched on 1990 June 1, and saw first light on 1990 June 16 (Trümper et al. 1991). After a two-month verification of the instrument operation it commenced its six-month long survey of the whole sky on 30 July 1990. During the RASS the observatory rotated about an axis through the sun, scanning on a given day a 2° wide strip passing through the ecliptic poles. The survey ended on 1991 February 18. The first analysis of the survey (RASS-1), which took place in 1991-1993, used data collected into the same 2° wide strips, and yielded a list of some 50,000 sources containing positions and such characteristics as count-rate, hardness ratio, angular extent and source detection likelihood. RASS-1 was used to test the algorithms implemented in the analysis and to start scientific studies, and as a consequence a series of improvements was initiated (Voges et al. 1999):

- i) Sorting the data into 1378 sky fields of size $6^\circ.4 \times 6^\circ.4$, overlapping at least 0.23° . This improved the efficiency of source detection.
- ii) For operational reasons the RASS-1 data base contained a few regions of low exposure, which were filled in later by supplementary observations. This later data was included in the RASS-2 data base.
- iii) Searching for sources in the soft ($0.1 - 0.4$ keV), hard ($0.5 - 2.0$ keV) and broad ($0.1 - 2.4$ keV) energy bands independently.
- iv) Refining the pointing attitude solution and improving source positions.
- v) Improvement of the spline-fit to the background, yielding more accurate source count-rates.
- vi) The list of candidates selected by the sliding-window source detection algorithms was increased by lowering the detection threshold, and in the subsequent maximum likelihood analysis the likelihood threshold for accepting sources was lowered from 10 (RASS-1 analysis) to 7.

Reanalysis of the survey data using the new software (RASS-2) was performed in 1994-1995, yielding a list of 145060 sources. The SGP field contained 11981 sources above a likelihood threshold of 7. The characteristics of the new software and results from the RASS-2 analysis have been described by Voges et al. (1999). The results described here

relied solely on the RASS-2 data base (RASS bright source catalog in Voges et al. 1999 and RASS faint source catalog in Voges et al. 2000).

The 2° wide RASS scan strips overlap to an extent which increases with ecliptic latitude, and consequently the exposure time grows and reaches a maximum at the poles. This effect is visible in the map of the RASS exposure time in the SGP survey region (Figure 1), in which there is a systematic increase from the NW to the SE corner. Upon this change are superposed striations caused by periodic protective shutdown of the focal-plane detector as it traversed radiation belts. Analysis of the exposure map of the SGP survey region yields the histogram shown in Figure 2, in which the mean exposure time is 300 seconds. There is an area of 75 sq deg in the SGP field, in which the exposure time is less than 10 s.

3.2 The COSMOS Data Base.

The ROE COSMOS digital data base contains the results of scanning 894 plates of the UK Schmidt IIIa-J (blue) southern hemisphere survey. The SGP study area contains 161 fields, each of size $5^{\circ}.35 \times 5^{\circ}.35$. COSMOS analyses and classifies each object in a field, and records the b_j magnitude, position (R.A. and declination (2000)) and object shape parameters. Objects are classified primarily as stars, galaxies or faint objects, the last being objects whose low intensity on the plate defies a reliable determination of their class. Heydon-Dumbleton, Collins, & MacGillivray (1989) compared the COSMOS galaxy number count-magnitude distribution with those derived from several independent optical surveys, and deduced that the galaxy sample was essentially complete (~ 95 percent completeness level) to a magnitude limit $b_j = 20.0$. Beyond this limit the star-galaxy discrimination gradually becomes less reliable as b_j increases (MacGillivray & Stobie 1985, Heydon-Dumbleton et al. 1989), leading to a significant incompleteness of the galaxy sample in the range $b_j > 20$. In the COSMOS data base star/galaxy separation was performed down to a limit of $b_j \sim 21.0$. An example of the results is given in a figure, which shows the ~ 20000 galaxies identified by COSMOS in the SGP field UKJ 411 (this figure is in the published article, but was too large for this archived version).

The galaxy magnitudes have been calibrated using photometric CCD observations of sequences of galaxies, which were used also in the calibration of the Edinburgh/Durham galaxy catalog (Heydon-Dumbleton et al. 1989). For any given plate COSMOS yields a galaxy intensity, which depends on such factors as exposure time, emulsion characteristics and measures taken to keep the plate in a dry environment during exposure. This implies that the galaxy magnitudes for any given plate must be adjusted to match the surrounding plates. This is done by identifying galaxies in the overlapping border zone of adjacent

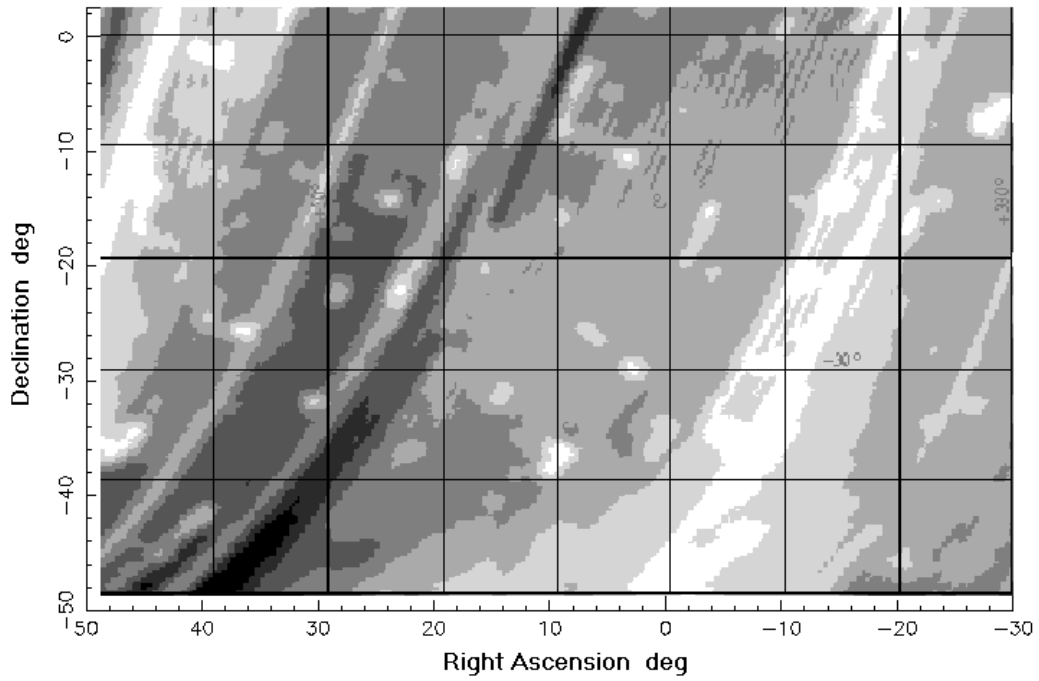


Fig. 1.— A map of the ROSAT survey exposure time distribution in the South Galactic Pole survey region. The increase toward the SE corner is a consequence of the procedure by which ROSAT scanned the sky (see text), and the striations are the result of shutting down the detector during passage through radiation belts.

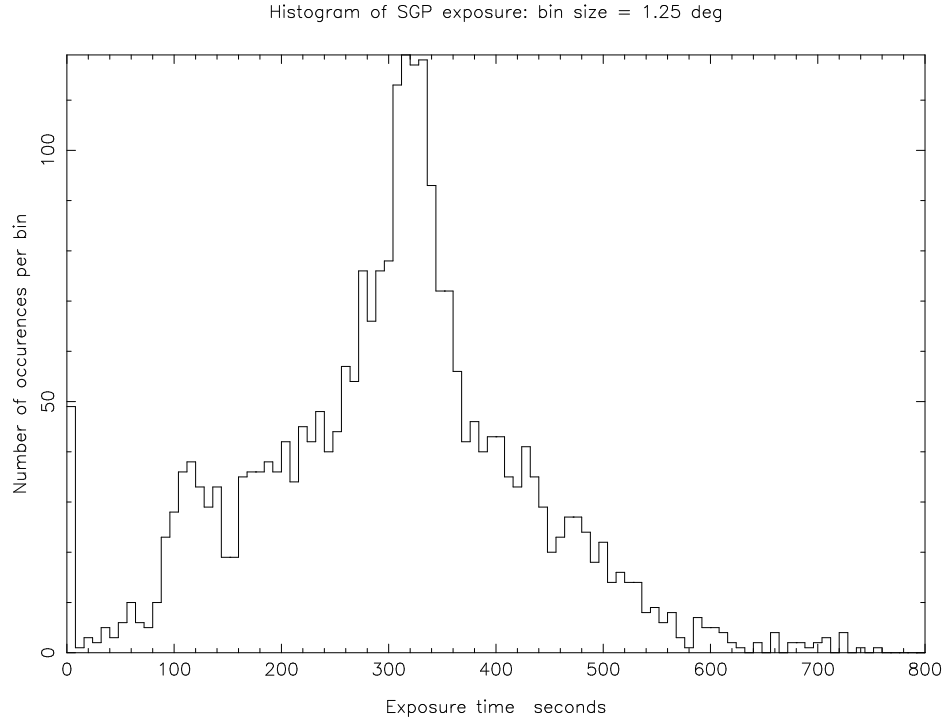


Fig. 2.— A histogram of the exposure times achieved in the SGP survey region, as displayed in the exposure map in Figure 1.

plates, and deriving a shift which matches the galaxy magnitudes. No unique solution for the whole southern sky is possible, and instead a set of plate magnitude shifts is obtained by a fitting procedure which globally minimises the inconsistencies between adjacent plates. The resulting 'COSMOS galaxy magnitudes' are on an arbitrary machine scale, which now must be adjusted to match the CCD calibrations, in essence providing a global zero point solution to the matched plate data. This is done by fitting a correlation between the CCD and COSMOS magnitudes of galaxies in the CCD observation sequences.

To further ensure there were no calibration problems as a result of the isophotal thresholding of the COSMOS galaxies (isophotal thresholding results in loss of light below the isophote level used and hence underestimation of the true brightness of a galaxy), we accepted for calibration purposes only galaxies in the COSMOS data which were at least three magnitudes above the plate limit (i.e. $b_j < 19.0$). This resulted in 207 sequence galaxies being accepted for calibration. The RMS scatter of the correlation between the COSMOS and the CCD magnitudes for these galaxies was found to be 0.25. As the intrinsic error in the CCD photometry is estimated to be 0.1 – 0.2, we estimate that the resulting error in the magnitudes derived for galaxies in the COSMOS IIIa-J southern hemisphere survey is ~ 0.2 .

Some independent corroboration of the COSMOS galaxy photometry is provided by the study of Caretta, Maia, & Willmer (2000). They confirm after comparisons with their CCD data that the COSMOS galaxy magnitudes are reliable at the ~ 0.2 level. Their results indicate that galaxy samples are 90 percent complete at magnitudes down to $b_j = 19.5-20.0$, in broad agreement with the COSMOS estimates. However this agreement should be treated with caution, as Caretta et al. (2000) studied a small area of sky having a lower galaxy count than is available in the UK Schmidt southern hemisphere survey.

3.3 CSEARCH: the Selection of Cluster Candidates.

The cluster search procedure (CSEARCH) counts galaxies within 5 circles of radius $R = 1.5, 3, 5, 7.5$ and 10 arcmin (circles 1 through 5), centered at the ROSAT source position, and compares the results with those of random sampling in the UKJ field. These radii correspond to the range of expected cluster core diameters (e.g. at $z \sim 0.3$ a radius of 300 kpc is equivalent to an angular scale of 1.1 arcmin and at $z \sim 0.03$ to 11 arcmin). The random sampling was performed 1000 times for each radius, yielding for each field five histograms of the galaxy count. For each histogram a table is created, giving the probability p that the galaxy count exceeds a value, N_g^* :

$$p = \frac{\sum_{N_g^*}^{\infty} n(N_g)}{\sum_0^{\infty} n(N_g)} \quad (1)$$

where n is the number of cases where the galaxy count was N_g . Selection of cluster candidates is made after setting a threshold $p = p_t$, which implies that for each plate a threshold be set for N_g^* . Individual plate sensitivity and statistics make this galaxy count threshold vary from plate to plate and yield a significant uncertainty. The following argument describes how this is circumvented by analysing the ensemble of probability values p for the whole SGP RASS-2 source sample.

The ROSAT source is accepted if the probability associated with one of the 5 galaxy counts (circles 1 through 5) at the ROSAT position falls below a selected threshold p_t . For convenience, we have defined and used the quantity $P = 1 - p$, as this approaches a maximum value of 1 for cluster candidates. The range $0 < P < 1$ is divided into bins of equal width (typically 400 in number), and for any given search radius R we create a histogram of the source count (n_x) per bin for all the RASS-2 sources in the SGP field. If there were no correlation between the ROSAT position and the galaxy count, as would be close to the truth for an ensemble of stars and AGN, the expectation value for the number of sources, n_x , per bin would be independent of P (Böhringer et al. 2001). Figure 3 shows the histograms of the probability P obtained for the ROSAT sources detected in the SGP region. To save space we show results for $R = 1.5, 3, 5$ and 10 arcmin only. The major characteristic of these histograms is indeed a flat distribution with statistical fluctuations, but in addition there is an enhancement at values of P approaching 1, which is the signature of clusters.

A comment on the data used to create these histograms is necessary. Following the first CSEARCH analysis of the SGP sources in the RASS-2 data base, examination of images overlaying the X-ray and the optical fields revealed multiple detections by RASS-2 of the more nearby clusters, due to their markedly extended X-ray emission (e.g. A119). This biases the CSEARCH analysis, and therefore we removed 256 redundant multiple detections from the RASS-2 SGP source list, and then repeated the analysis. This number is small compared to the total of 11981 sources, but is more significant in relation to the size of the eventual CSEARCH sample of cluster candidates (3236).

The threshold P_t must be chosen carefully in terms of the desired compromise between formal completeness C_o and contamination C_t , for inevitably the selected sample contains ROSAT sources having chance associations with concentrations of galaxies, which build the flat distribution, and so the price of higher completeness is an increased contamination. The probability threshold P_t is related to C_o and C_t by the following equations:

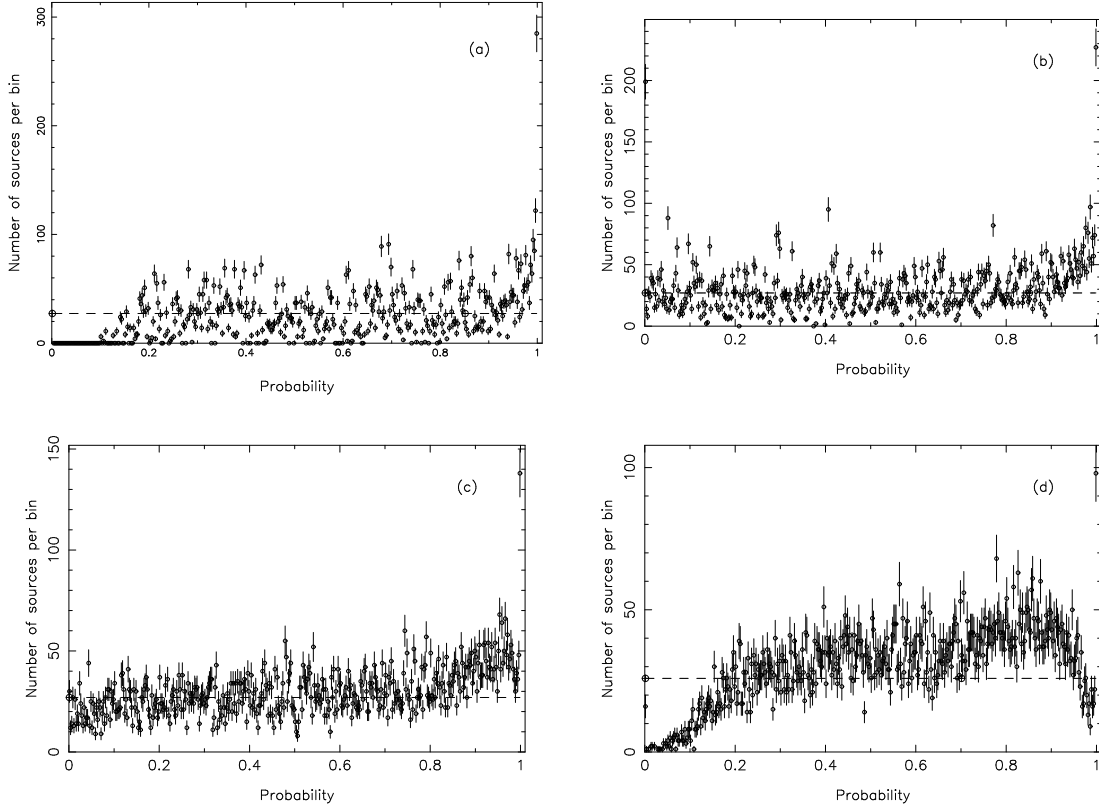


Fig. 3.— The CSEARCH analysis counts galaxies within a circle of specified radius centered on the ROSAT source position, compares this with the results of 1000 random samplings over each UK Schmidt field, and computes a probability p that the measured count is a statistical fluctuation of the background. We define a quantity $P = 1 - p$ which tends to 1 in dense galaxy concentrations. and divide the range $0 < P < 1$ into 400 bins of equal width. The four plots show the distributions of source count per bin, using all ROSAT sources in the SGP region, obtained using circles of radius (a) 1.5, (b) 3, (c) 5 and (d) 10 arcmin.

$$C_o = \frac{\sum_{P_t}^1 (n_x - n_b)}{\sum_0^1 (n_x - n_b)} \quad (2)$$

$$C_t = \frac{\sum_{P_t}^1 n_b}{\sum_{P_t}^1 n_x} \quad (3)$$

where n_b is the number of sources per bin in a specified flat portion of the probability histogram.

Before the results of CSEARCH are discussed, two characteristics of the histograms shown in Figure 3 should be clarified. First, the dip in P for circle 1 in the range $0 < P < 0.15$ is a quantisation effect, due to the galaxy count jumping from 0 to 1. The dip for circle 5 in the same region appears to be due to sampling limits, resulting from the circle diameter being a significant fraction of the field width. We have examined the number density of clusters found in our analyses as a function of position on the plate, and have found no sign of incompleteness near the COSMOS digitisation boundaries on the plate.

Second, whereas the histograms for circles 1 and 2 decay rapidly from the peak at $P \sim 1$ to a flat plateau, those for circles 3 and 5 decay even more rapidly to a minimum and then rise to a second enhancement in P , covering the range $0.8 < P < 0.97$ for circle 3 and $0.7 < P < 0.9$ for circle 5. To search for the cause of this second enhancement we examined how candidates found using circles 1 and 2 were registered using circles 3 through 5. A typical result (Figure 4) shows how compact groupings of galaxies found by circle 2, for which $0.95 < P < 1$, are detected using circle 5. The number of sources falls sharply from $P = 1$ to a minimum, rises to a peak at $P \sim 0.92$ and then falls again gradually, i.e. much of this second enhancement is due to relatively compact groups, for which the number of galaxies counted is not significantly enhanced when detected with circles 3 and 5. As a consequence the effect of increasing the circle radius is to reduce P .

The five candidate lists ($R = 1.5, 3, 5, 7.5$ and 10 arcmin) are cross-correlated to remove redundant detections, and so this second enhancement is in principle not a problem. However, if for each circle P_t is set so as to yield a high value of C_o (equation 2), then for circles 3 through 5 the contamination C_t is increased substantially, making the subsequent screening of the sample more difficult and time-consuming. Therefore as a precaution, for circles **4 and 5 only** we have set P_t at 0.95, so as to include only the sharp peak. We show below that this is a reliable procedure.

The SGP field contains 11981 RASS-2 sources having a likelihood greater than or equal to 7. Table 1 shows the results of analysing this sample with CSEARCH, and summarises the assumptions made in selecting cluster candidates. The last entry N_{new} gives the yield of new candidates as one starts with circle 1, and then proceeds from circles 2 to 5, **removing**

redundant detections at each stage. The trends in these numbers confirm the expectation that the smaller circles should detect the majority of clusters. The decision to set P_t to 0.95 for circles 4 and 5 was supported later by a search of the final list of 186 cluster candidates, which revealed no case in which the CSEARCH detection relied solely on circle 4 and/or circle 5. The total sample extracted using CSEARCH comprised 3236 candidates. Table 1 indicates that the majority of clusters are detected using circles 1, 2 and 3, and we deduce from column 6 that the contamination of the sample should lie between 46 and 56 percent.

3.4 Reanalysis of the X-ray Data using the Growth Curve Analysis (GCA)

Previous studies found that the energy flux from extended sources is underestimated by the standard RASS source detection algorithm (Ebeling et al. 1996, 1998 and De Grandi et al. 1997), and section 2 has stated the various analyses developed to correct this problem. The growth curve analysis (GCA) method, described in detail by Böhringer et al. (2000), has been used in this study to analyse the RASS-2 data base. The GCA returns among other information the following important parameters: background subtracted source count-rate and its Poisson (photon statistical) error, a locally redetermined position of the centroid of the source X-ray emission, the mean exposure for the source region, a significance of the source detection, the radius out to which source emission is significantly detected, a hardness ratio characterizing the source spectrum and its photon statistical error, a fitted source core radius, and the probability, obtained using a Kolmogorov-Smirnov test, that the object is consistent with being a point source. The source position is determined with an error which in most cases is less than 1 arcmin, the exceptions being nearby clusters with irregular emission structure. Errors in count-rate and hardness ratio are given in our catalog (Table 3). Taking A2726 as an example, the hard band count-rate is $0.103 \pm 0.022 \text{ ct s}^{-1}$ and the hardness ratio is 0.43 ± 0.27 .

The basic parameters are derived from the photon distribution using the three energy bands ‘hard’ (0.5 to 2.0 keV, channel 52 - 201), ‘broad’ (0.1 to 2.4 keV, channel 11 - 240), and ‘soft’ (0.1 to 0.4 keV, channel 11 - 40). The band definitions are the same as those used in the standard analysis (Voges et al. 1999). Most of the derived parameters are based on analyses of data in the hard energy band, as clusters are detected in this energy band with the highest signal-to-noise ratio. One of the exceptions is the hardness ratio, which requires also the results from the soft band.

The GCA method uses the photon event distributions in two circles (Figure 5), of radii 20 and 41.3 arcmin, centered initially on the RASS-2 source center. Events within the inner

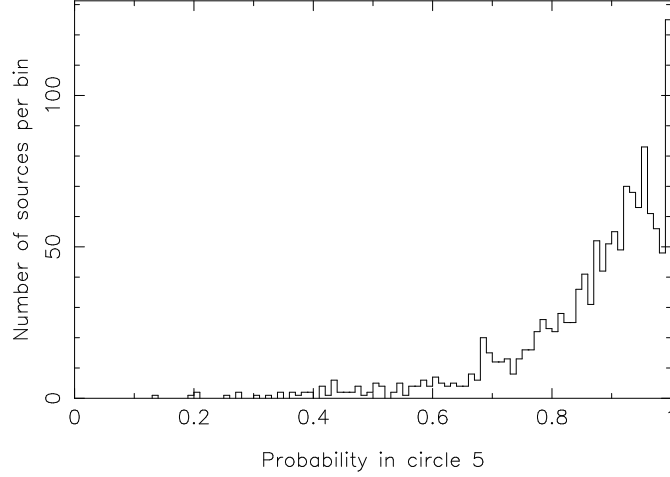


Fig. 4.— Galaxy concentrations yielding a high value of the statistic P for CSEARCH circles of small radius yield lower values when larger radii (R) are used, and so produce a secondary peak in the P-distribution. The plot shows this distribution for a circle of $R = 10$ arcmin, taking as a sample SGP sources obtained using $R = 3$ arcmin and for which $0.95 < P < 1$.

Table 1. Summary of the CSEARCH Analysis of the RASS Sources in the SGP Region.

Circle	Circle radius arc min	P_t	Range for estimating n_b	Completeness C_o	Contamination C_t	N_{new}^a
1	1.5	0.92	$0 < P < 0.85$	0.925	0.46	1857
2	3	0.90	$0 < P < 0.85$	0.900	0.50	884
3	5	0.90	$0 < P < 0.80$	0.700	0.56	428
4	7.5	0.95 ^b	$0 < P < 0.70$	-	> 0.75	33
5	10	0.95 ^b	$0 < P < 0.70$	-	> 0.75	34

^aAfter removal of sources found using circles of smaller radii.

^bProbability threshold set to include only the sharp peak in the P-distribution (see text). The completeness and contamination are difficult to estimate due to the gradient in the P-distribution.

circle are analysed to determine the source characteristics, and those in the outer annulus are used to determine the background level. In some cases special analyses were necessary, where either clusters had an unusually large angular extent, or where two or more sources lay in a confused region, requiring the use of 'deblending' algorithms.

The source count-rate is determined from the cumulative, radial source count rate profile ('growth curve') after background subtraction. The construction of the growth curve is preceded by a redetermination of the source center and by the background measurement. A typical example for the resulting growth curve is displayed in Figure 6, showing the count-rate plotted as a function of integration radius (solid curve). The dashed lines show the limits determined by applying the photon event statistical error (including the error for the background subtraction).

The count-rate is determined in two alternative ways. In the first a significant outer radius of the source is defined as the point where the increase in the 1σ error is larger than the increase of the source signal. The integrated count-rate is calculated using events within this 'cutoff' radius. In the second method a horizontal level is fitted to the outer region of the plateau, and this value is adopted as the standard in quoting hard-band X-ray count-rates and in calculating cluster energy flux and luminosity (section 4). However, we use the first method also as a check on the count-rate and as a means of estimating systematic uncertainties in the count-rate determination, which must be combined with the pure photon statistical errors.

Careful examination of the overlays of X-ray and optical images (section 3.5.1) of the cluster sample revealed 19 cases in which the source was very extended, or source confusion might cause errors in deriving the source count-rate. These 19 were subjected to the special analyses referred to above, in which the source count-rates were revised. Six systems were identified as double clusters and not subjected to the deblending analysis. They are identified as double clusters in the survey catalog (Table 3).

The other two important source properties determined by the GCA method are the spectral hardness ratio and the source extent. The hardness ratio, HR, is defined as $HR = \frac{H-S}{H+S}$ where H is the hard band and S the soft band source count-rate (both determined for the same outer radius limit).

The source extent is investigated in two ways. In the first a β -model profile (Cavaliere & Fusco-Femiano 1976) convolved with the averaged survey PSF is fitted to the differential count-rate profile (using a fixed value of $\beta = 2/3$), and we derive from the results a core radius, r_c . In the second a Kolmogorov-Smirnov (KS) test is used to estimate the probability that the object is a point source. It is taken as highly likely that the source is extended when

1RXSJ020144.2-021158

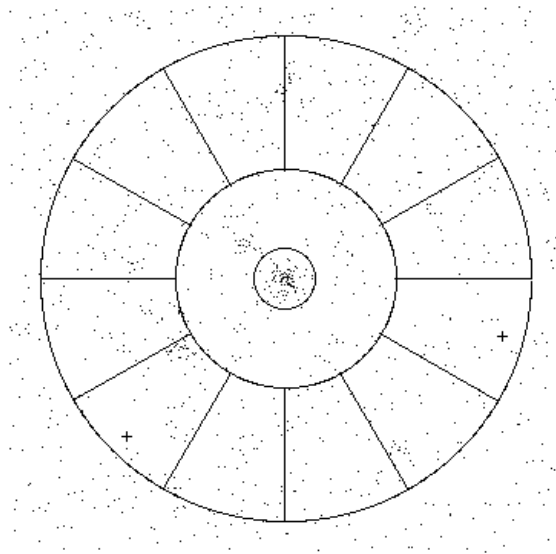


Fig. 5.— The configuration used in the growth curve analysis (GCA) of a ROSAT source. The image shows the distribution of photon events in the hard band (0.5 – 2.0 keV) within a square field of width 1.5 deg, centered on the source to be studied. The background is measured in the annulus between the two outer circles of radii 20 and 41.3 arcmin, which is divided into 12 sectors. A sector is discarded if its background has too high a deviation from the average. Two examples are marked with a cross. The small inner circle designates the radius out to which significant X-ray emission was detected by the GCA for this source.

the KS probability is less than 0.01. Tests with X-ray sources which have been identified with stars and AGN showed that a false classification as an extended source occurred in less than 5% of the sample.

The final step in the X-ray analysis was to establish a lower limit to the source count-rate, in order to set practical limits to source identification and redshift determination. The list of 3236 candidates from the CSEARCH analysis (section 3.3) was truncated using a threshold of 0.08 cts^{-1} for the cut-off radius count-rate in the hard band. This reduced the list of candidates to 477. A sharp limit in count-rate corresponds to a range of energy flux, determined by the variation of interstellar column density (N_H) in the field, which leads to some incompleteness at low fluxes. Böhringer et al. (2001) estimate a range of $1.55 - 1.95 \cdot 10^{-12} \text{ erg s}^{-1}$ in the band $0.1 - 2.4 \text{ keV}$ for $10^{20} < N_H < 10^{21} \text{ cm}^{-2}$. In the SGP field N_H takes on relatively low values so that, for example, for only 8 percent of the clusters selected is $N_H > 4.0 \times 10^{20} \text{ cm}^{-2}$. Therefore we can be certain that this source of incompleteness is absent at fluxes greater than $2 \cdot 10^{-12} \text{ erg cm}^{-2} \text{ s}^{-1}$.

3.5 Removal of Contaminating Sources from the Cluster Candidate List.

The removal of contaminating sources from the list of 477 candidates was by necessity an iterative process, in which the decisions made were reviewed repeatedly to ensure that the criteria used had been applied consistently. The following sections describe the steps in this process.

3.5.1 Examination of COSMOS Finding Charts and Overlays of X-ray and Optical Fields.

For each cluster candidate a finding chart $7 \times 7 \text{ arcmin}^2$ in size was extracted from the COSMOS data base. In addition an overlay was made of the X-ray surface brightness contours upon the COSMOS optical field. For example Figure 7 shows the overlay made for the Abell cluster A3854. Examination of these finding charts and overlays during the selection process has been valuable for several reasons. First, visual scrutiny has removed cases in which CSEARCH had been deceived by artifacts, for example satellite trails, the haloes and diffraction spikes of bright stars, and the attempt by COSMOS to resolve the structure of bright nearby galaxies. These structures often were resolved by COSMOS into objects identified as galaxies. Second, the RASS-2 analysis resulted in multiple detections of extended sources such as clusters, which may be removed after examination of the X-ray/optical over-

lays. As described in section 3.3, a significant number of redundant detections was removed to minimise any bias of the CSEARCH analysis. However this process was not perfect, and it was possible later to identify further cases by careful re-examination of the overlays. The latter are counted in the detection statistics shown later in Table 2. Finally, scrutiny of the finding charts and overlays has identified occasional errors, which are simple to correct, where a CSEARCH candidate is identified with a faint RASS-2 X-ray source having a brighter X-ray neighbour. The GCA technique then has preferred the latter and derived the higher count-rate. This problem was detected through visual examination of the overlays.

3.5.2 Rejection Criteria based on X-Ray Hardness Ratio and Angular Extent.

The temperature and extent of the hot gas in clusters of galaxies make it possible to set limits to both the X-ray hardness ratio and the angular extent of a RASS cluster source (Ebeling et al. 1996, 1998). This provides effective discriminants between clusters and the majority of contaminating sources in the CSEARCH sample, made up of AGN and stars. In this section we justify the following two criteria, which have been used in removing a large fraction of these contaminating sources:

- 1) The **upper limit** of the X-ray hardness ratio (section 3.4) is less than zero, i.e. if $HR_{ul} < 0$, the source is too soft.
- 2) The core radius r_c obtained from the angular extent calculation is less than 0.5 arcmin, i.e. the object is a point source.

These criteria were applied independently in rejecting sources. In order to establish criteria using these parameters, we selected control samples describing the characteristics of clusters, AGN and stars. The first contained 118 Abell clusters extracted from the total sample of 477 candidates (section 3.4), using as a criterion a correlation between the X-ray position and the centroid of an Abell cluster. Conservatively we excluded from the sample clusters where the separation between the ROSAT and Abell positions was greater than 5 arcmin, where the survey exposure was low (< 100 s), or where X-ray maps revealed nearby components in the source region, one of which might not be a cluster. In each case the X-ray/optical overlay image (section 3.5.1) and the COSMOS finding chart were examined. The count-rates of these clusters covered the full range of the study reported here.

The second and third control samples comprised AGN and stars detected by the ROSAT survey and identified through spectroscopic optical observations. This project was a collaboration between MPE and ESO, in which the error circles of all RASS-1 sources in four relatively small regions of the southern hemisphere were searched using the COSMOS data base to identify optical candidates. The nature of these candidates was examined through

spectroscopic observations, after which the likely source of the X-ray emission was identified (T. A. Fleming 1994, private communication). Using three of these fields having a total area of 570 sq deg, we selected samples of 138 AGN and 61 stars, whose positions are within 20 arcsec of the RASS-2 source positions. Again, the X-ray count-rate of these sources covered the full range of the cluster survey reported here.

The hardness ratio (HR) distributions for these samples are shown in Figure 8. Whereas $HR > 0$ for 97 percent of the Abell clusters in our test sample, $HR < 0$ for 53 and 51 percent of the AGN and star samples respectively. Therefore a conservative threshold of zero for the **upper limit** to HR has been set, above which RASS sources qualify for retention in the list of cluster candidates. This is an effective method of removing a large fraction of the stars and AGN in our sample of 477 candidates.

The angular extent, as measured by the derived core radius r_c , provides an effective test for distinguishing clusters from AGN, which however runs into two difficulties. The first is caused by the diminishing size of clusters with increasing redshift, an effect which is emphasised if the cluster contains a cooling flow. The second is the effect of source confusion in a RASS-2 detection of an AGN, when the GCA analysis may yield a finite value for the source extent. These difficulties are constrained to a certain extent by the redshift limit ($z \sim 0.3$) and by the limit set to the X-ray count-rate in the hard band (section 3.4). The distributions of r_c derived from the two samples are shown in Figure 9. The rise in these curves at a radius of 6 arcmin is a result of setting a limit $r_c \leq 6$ arcmin in the GCA, and to a lesser extent of the influence of surrounding sources on the growth curve analysis (section 3.4). The important characteristic is that 58 percent of AGNs satisfy $r_c = 0$, whereas 97 percent of Abell clusters in our test sample satisfy the condition $r_c \geq 0.5$ arcmin. Therefore only those sources among the 477 CSEARCH cluster candidates were retained which satisfied the condition $r_c \geq 0.5$ arcmin. As discussed in section 3.5.5, this results in some incompleteness near the survey limit, where the RASS and COSMOS data become marginal in the detection of distant clusters.

We have examined four clusters in the Abell control sample, which were rejected when these hardness ratio and core radius criteria were used. One, associated with A2800, failed the hardness ratio test. This may be due to contamination, as it is in a confused region of X-ray emission. Three sources, associated with A3866, S181 and S1121, failed the core radius test. In the case of S181 the galaxies are faint and displaced from the center of the X-ray source, which is comparatively strong (0.134 ct s^{-1} in the hard band). The small RASS-2 error circle contains a stellar object ($b_j = 17.7$), and therefore we conclude that this source is an AGN (the emission from AGN comes from a concentrated region, so that often COSMOS classifies the object as a star). The source coincident with A3866 has a high count-rate

(0.4 cts^{-1}) yet shows only weak signs of extent. Although the spectroscopic observations (Romer 1995) revealed evidence of an AGN, overlaying an EINSTEIN HRI image upon an optical DSS image indicates that the central object is probably a cD galaxy and that the X-ray source is very compact but not a point source. Thus the decision to reject this source is open to correction. S1121 appears to be an example of a distant cluster near the limit of the survey sensitivity. Thus four clusters in the test sample of 118 Abell clusters were rejected, from which we estimate that in applying the hardness ratio and core radius criteria to our cluster sample, the loss of clusters should be less than 4 percent.

3.5.3 Removal of Bright Stars.

Bright stars appear in the sample of cluster candidates either because of a chance association with a region of high galaxy density, or because COSMOS has broken down the diffraction spikes and/or halo into objects classified as galaxies. They have been removed using two tests, one being the hardness ratio test described in section 3.5.2 and one being a statistical test. In the latter we have analysed 17 regions of diameter 1° in the SGP field, using the COSMOS data to derive the mean density of stars as a function of b_j magnitude. The following argument was used to reject RASS-2 sources having stars brighter than $b_j = 12$ in the error circle. The density of stars brighter than $b_j = 12$ was found to be $0.0165 \text{ arcmin}^{-2}$, which implies that the probability of finding such a star by chance in a RASS-2 90-percent confidence error circle, which typically has a radius of about 30 arcsec, is 0.013. Therefore if we reject all candidates having a star brighter than $b_j = 12$ within the error circle, the loss of clusters from the sample should be no more than 1 – 2 percent.

This procedure has been applied by correlating the candidate list with stars in the SIMBAD and TYCHO (Høg et al. 1998) catalogs. A correlation of the b magnitudes in these catalogs with the COSMOS b_j magnitudes shows that the latter are lower by about 0.5 magnitudes for stars fainter than $b_j \sim 10$, but that the difference widens steadily for brighter stars. Therefore in examining bright SIMBAD or TYCHO catalog stars in the RASS-2 error circle we set a threshold of $b = 12.5$, below which the star was judged to be the cause of the X-ray emission.

Additional stars, not listed in the SIMBAD and TYCHO catalogs, were identified later by inspection of the COSMOS finding charts and the X-ray/optical overlay images for the 477 candidates.

3.5.4 Removal of AGN and Large Extended Emission Regions.

The X-ray sources removed by the hardness ratio ($HR_{ul} < 0$) and core radius ($r_c < 0.5$ arcmin) tests have been reviewed carefully, using correlations of the list of 477 candidates with the Veron Catalog of active galaxies (Veron-Cetty & Veron 1998) and the NASA Extragalactic Data Base (NED) to identify sources for which the 90 percent RASS-2 error circle contained an identified AGN, and examination of the X-ray/optical overlay images and the COSMOS finding charts. However in the sample remaining after these tests, after removal of stars (section 3.5.3) and after identification of detections resulting from COSMOS artifacts, there remained a contaminant comprising 28 sources for which $HR_{ul} \geq 0$ or $r_c \geq 0.5$ arcmin, but whose identification as a cluster was suspect. These sources were reviewed using again the Veron and NED correlations, overlay images and COSMOS finding charts, but in addition using the results of the CSEARCH analysis. Of these 28 we rejected 9 as being AGN and 1 as an X-ray source superposed on a nearby galaxy over 5 arcmin in extent. Nine sources were excluded because the extent detection was due to source confusion, and 8 because CSEARCH either made an identification at a large radius only, inconsistent with the small X-ray extent, or made an error due to COSMOS artifacts. The one remaining source requires further study and was rejected tentatively. There is a possible association with A2813, but the minimum found by GCA in the core radius fit was very shallow and the evidence for a cluster in the X-ray/overlay image was indecisive.

The total number of AGN identified was 127, and Figure 10 shows the distribution of their b_j magnitudes, as measured by COSMOS. Where the AGN was not identified in the Veron catalog or NED, b_j for the brightest object inside the 90 percent error circle was used. The half-width of the distribution lies in the range $15 < b_j < 19$.

Finally, we discovered five candidates showing large extended regions of X-ray emission 10 – 20 arcmin in diameter, whose optical fields show no signs of a significant galaxy population and whose origin as the confusion of several sources is not obvious.

3.5.5 Summary of the Selection Statistics and Estimate of the Sample Completeness.

After removal of RASS-2 sources contaminating the SGP sample of 477 cluster candidates, using the procedures described above, there remained 186 candidates. The statistics of this selection process are summarised in Table 2. Of the 61 redundant RASS-2 detections in Table 2 which eluded the earlier screening, 24 were associated with clusters. Therefore of the 477 candidate sources $N_{eff} = 210$ are associated with clusters, which implies that the

contamination of the sample of 477 was 0.56. This is in marginal agreement with the results of the CSEARCH analysis (section 3.3), which predicted $0.46 < C_t < 0.56$. Examination of Table 1 shows that 84.7 percent of the cluster candidates were identified by CSEARCH using the smaller circles 1 and 2, and consequently that formally the contamination of the sample should be 0.5 or less, and the completeness about 0.90. Therefore we can estimate that the sample of 477 candidates should contain $0.5 \times 477 = 238$ clusters and that a complete sample obtained using CSEARCH would have yielded $N_{tot} = 0.5 \times 477 / 0.9 = 265$ clusters. Therefore we can estimate that the overall completeness of the sample of selected clusters is $N_{eff} / N_{tot} = 210 / 265 = 0.79$. This incompleteness, which is the sum of the three effects summarised in section 2, contributes to the flattening of the $\log N / \log S$ distribution at fluxes below $3.0 \times 10^{-12} \text{ erg cm}^{-2} \text{ s}^{-1}$ in the band 0.1 – 2.4 keV (section 5).

The above argument implies that $238 - 210 = 28$ clusters have been missed in searching the 477 candidates. This has arisen in most cases while applying the criteria $HR_{ul} < 0$ and $r_c = 0$ to reject candidates, and in section 3.5.2 we have estimated that applying these criteria applied to a control sample of Abell clusters should yield an incompleteness of 4 – 5 percent. Two examples of clusters with overly soft spectra are A2800 ($HR = -0.15 \pm 0.11$) and the cluster 2310 – 73 ($HR = -0.19 \pm 0.13$) discovered by Tucker et al. (1995) in the EMSS. In neither case is the nature of the contaminating source clear.

One limit of this study is that the criterion $r_c \geq 0.5$ arcmin for selecting cluster candidates will inevitably discriminate against the more distant clusters of small angular extent, particularly those in which a cooling flow makes the X-ray source more compact. This loss is evident in the flattening of the $\log N$ - $\log S$ distribution at low flux (section 5). Three aspects of the analysis bear out this trend. First, of the sources rejected because $r_c = 0$ we identified at least 4 cases, where the X-ray/optical overlays showed suggestive but marginal evidence that they were clusters. Second, there were 11 in our catalog of 186 clusters, for which the detection of angular extent appeared to be near its limits. The GCA yielded a small but non-zero core radius, but simultaneously the KS-test yielded significant probabilities, between 10 and 50 percent, of the source being point-like. Third, in the case of distant clusters accepted by CSEARCH, COSMOS classified some of the galaxies as ‘faint objects’, which the CSEARCH analysis did not count. This is obvious in some of the X-ray/optical overlays of these objects, which show the dominant elliptical galaxy with halo surrounded by faint objects. Therefore we conclude that some distant clusters may have been missed by CSEARCH.

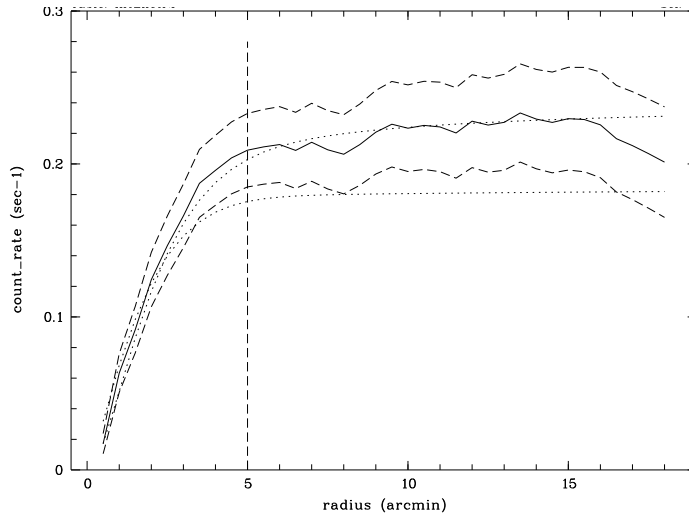


Fig. 6.— Integrated count-rate profile for the source shown in Figure 5. The integrated count-rate profile is background-subtracted and the two dashed curves give the limits determined by the 1σ statistical error, which includes the uncertainties of the signal and the background determination. The vertical dashed line shows the outer source radius, as defined in the text. The lower dotted curve shows the χ^2 fit of a point source to the data, and the upper one shows the best King-model fit.

Table 2. Summary of the Results of Analysing the Sample of RASS-2 Cluster Candidates in the SGP Region.

Source	Number
Clusters of galaxies	186
Active galactic nuclei (AGN)	127
Stars	74
Extended X-ray emission regions	5
Redundant RASS-2 detections	61
Sources below X-ray count-rate threshold	24
Total	477

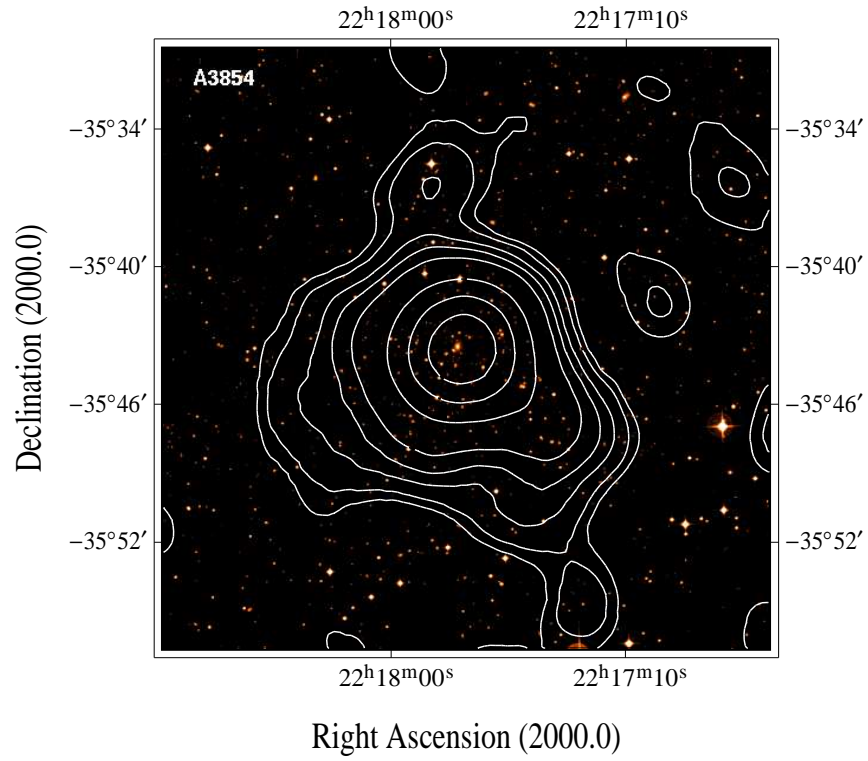


Fig. 7.— A contour plot of the X-ray flux from A3854 in the hard band (0.5 – 2 keV), superposed on the COSMOS digitised image obtained from the UK Schmidt IIIa-J survey

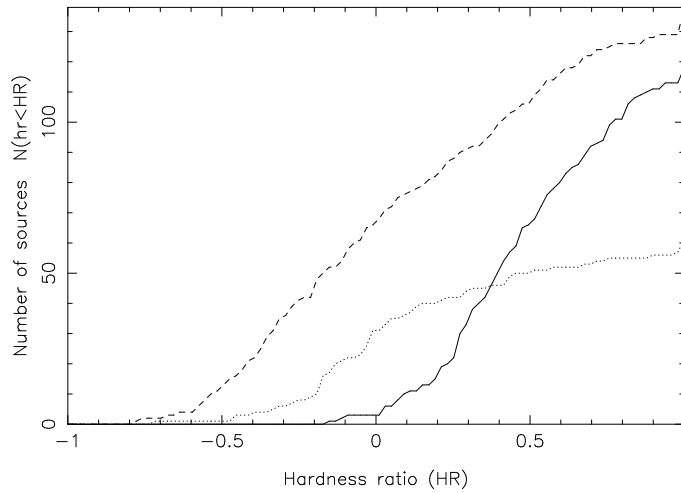


Fig. 8.— The cumulative distributions of hardness ratio for selected samples of ROSAT sources are shown by the dashed line for AGN and by the dotted line for stars. The samples comprise all RASS sources in three special fields selected for an ESO Key Project (not the Key Project described in the text in regard to cluster redshift determination), which were identified by spectroscopic optical observations. The solid line is the distribution for an unambiguously identified sample of Abell clusters of galaxies in the SGP region.

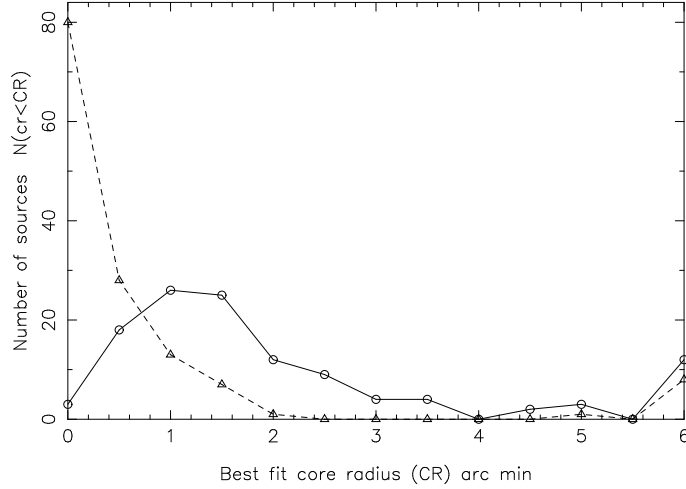


Fig. 9.— The distributions of core radius obtained by fitting a King model for cluster surface brightness distribution to the samples of AGN and clusters used in deriving Figure 8. AGN are represented by the dashed line and clusters of galaxies by the solid line. The rise in the distributions near a core radius of 6 arcmin is discussed in the text.

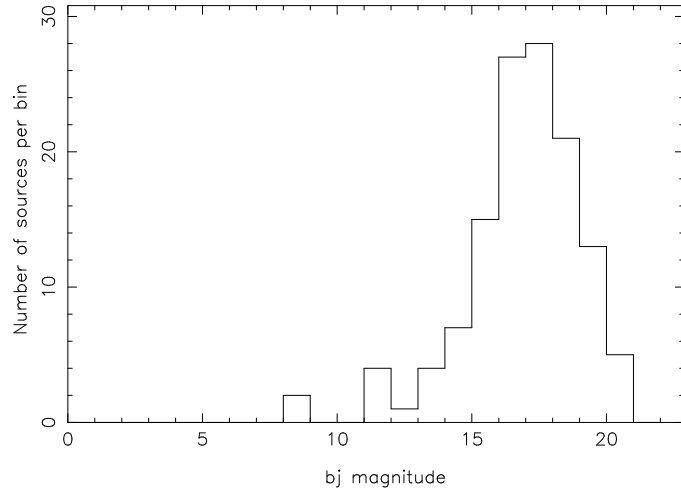


Fig. 10.— The distribution of b_j magnitude for the sample of sources identified in the SGP region as AGN.

4. CLUSTER X-RAY ENERGY FLUX AND LUMINOSITY

In order to convert the ROSAT count-rate into an energy flux outside the galaxy, the spectrum of the hot intracluster medium (ICM) has been convolved with the response functions of the interstellar medium (ISM) and the instrument. The plasma emissivity was derived using the version of the Raymond & Smith (1977) code installed in 1994 in the MPE EXSAS software. The technique has been verified by comparing results with those obtained using the EXSPEC analysis code (Böhringer et al. 2000). The cluster plasma was assumed to contain elements heavier than hydrogen having abundances 0.35 times the solar abundance. The HI column densities used in calculating the ISM absorption have been taken from Dickey & Lockman (1990). These calculations have been made over ranges of temperature between 0.05 and 10 keV (5.8×10^5 - 1.16×10^8 K), and of HI column density between 10^{19} and 10^{22} cm⁻². The resulting matrix was used to convert the count-rate in the hard band to an energy flux f_x in units of erg cm⁻² s⁻¹ in the 0.1-2.4 keV band.

For each cluster whose redshift has been measured the X-ray luminosity has been calculated using the relations:

$$L_x = K f_x 4\pi D_L^2 \quad (4)$$

$$D_L = \frac{c}{H_0 q_0^2} (q_0 z + (q_0 - 1)((2q_0 + 1)^{1/2} - 1)) \quad (5)$$

where L_x is the luminosity in the 0.1-2.4 keV band, K is the correction for redshifting of the radiation, and D_L is the luminosity distance. K has been calculated for ranges of redshift between 0.025 and 0.5, and of ICM temperature between 0.05 and 10 keV. The resulting matrix was used to convert energy flux into luminosity.

Measured cluster temperatures have been taken from the compilation in Table 1 of White et al. (1997). Where measured temperatures have not been found we have used the luminosity-temperature correlation derived by White et al. (1997):

$$L_{bol} = 0.0478 T^{2.98} \quad (6)$$

where L_{bol} is the X-ray luminosity in the 0.01-80 keV band and T is the temperature in keV. The assumed temperature was used to calculate a bolometric correction to the luminosity. For each source a cycle of iterations was performed in the flux and luminosity calculations, until the change in temperature fell below 1 percent. Where neither redshift nor temperature has been measured, we have assumed a temperature of 5 keV.

5. RESULTS OF THE SGP CLUSTER SURVEY

The procedures described in sections 2, 3 and 4 for searching the RASS-2 data base for cluster candidates, selecting clusters from this sample and determining their X-ray characteristics, have resulted in the catalog of 186 clusters shown in Table 3. The following notes, listed by the column number in the table, augment the information given in the header to each column.

- (1) ROSAT X-ray source name.
- (2) Right ascension (h:m:s J2000) of the centroid (GCA) of the cluster X-ray emission.
- (3) Declination (d:m:s J2000) of the centroid (GCA) of the cluster X-ray emission.
- (4) Count-rate in cts s^{-1} in the hard band (0.5 – 2.0 keV), with error (GCA).
- (5) X-ray hardness ratio, with error (GCA).
- (6) Total ROSAT survey exposure time for the cluster, in seconds.
- (7) Column density of interstellar atomic hydrogen at the cluster center, in units of 10^{20} cm^{-2} .
- (8) Temperature of the cluster gas, derived by the procedure described in section 4, in keV. The superscript 'e' indicates that no measurement was found, and the temperature was determined using an $L_{bol} - T$ correlation. Where no redshift was available a temperature of 5 keV was assumed.
- (9) Energy flux from the cluster, with the absorption by galactic interstellar absorption removed. The units are $10^{-12} \text{ erg cm}^{-2} \text{ s}^{-1}$ in the 0.1 – 2.4 keV band.
- (10) X-ray luminosity of the cluster in its rest-frame, derived using the procedure described in section 4. The units are $10^{44} \text{ erg s}^{-1}$ in the energy band 0.1 – 2.4 keV. We assume $H_0 = 50 \text{ km s}^{-1} \text{ Mpc}^{-1}$ and $q_0 = 0.5$.
- (11) Optical identification of the cluster. The meaning of the prefix to the identification and the appropriate reference are given in Table 4. For five sources identified as double clusters, the label 'dc' has been appended to the identification.
- (12) Redshift of the cluster.
- (13) Label for the reference from which the redshift was obtained:
 1. Romer (1995) 2. H. Böhringer and L. Guzzo 1999, ESO Key Project, private communication) 3. Struble & Rood (1999) 4. Katgert et al. (1996) 5. Quintana & Ramirez (1995) 6. Fetisova et al. (1993) 7. De Grandi et al. (1999) 8. H. Andernach 1989, "A Compilation of Measured Redshifts of Abell Clusters", unpublished, private communication 9. Crawford et al. (1995) 10. Huchra et al. (1999) 11. Shectman (1985) 12. Mazure et al. (1996) 13. Collins et al. (1995) 14. Dalton et al. (1997) 15. De Vaucouleurs et al. (1991) 16. Stocke et al. (1991) 17. Postman et al. (1992) 18. Abell, Corwin, & Olowin (1989) 19. Katgert et al. (1998) 20. Ebeling & Maddox (1995) 21. Muriel, Nicotra, & Lambas (1995) 22. Shectman et al. (1996) 23. Lauberts & Valentijn (1989) 24. Da Costa et al. (1998) 25. Dalton, Efstathiou, & Sutherland (1994) 26. Di Nella et al. (1996) 27. Ratcliffe et al.

(1998) **28**. Given in NED, reference uncertain.

(14) Number of galaxy redshifts used in deriving the cluster redshift.

Images of these clusters, showing overlays of the hard band X-ray contours upon optical images reconstructed from the COSMOS digital data base, are accessible over the Internet at (<http://wave.xray.mpe.mpg.de/publications/papers/2001/RASS-SGP-clusters/xray-optical-images>). They comprise 134 Abell clusters, 15 clusters found in other catalogs, and 37 newly discovered clusters. The number of Abell clusters in the SGP survey area is 1215, including 332 southern supplementary clusters, Therefore the Abell clusters in the SGP catalog (Table 3) comprise 11.0 percent of all Abell clusters in the SGP survey area. The Abell fraction of the SGP cluster sample (72%) is in good agreement with that of the BCS (Ebeling et al. 1999, 2000). We have compared the catalog in Table 3 with the REFLEX catalog of bright clusters published by De Grandi et al. (1999), which contains 54 clusters lying in the SGP region. Applying their energy flux threshold of $5 - 6.6 \times 10^{-12} \text{ erg cm}^2 \text{ s}^{-1}$ in the 0.1 – 2.4 keV band to Table 3, we find all but one cluster from the list of De Grandi et al. (1999). The exception is A3866, which we have rejected tentatively as a source whose X-ray flux may be dominated by an AGN (section 3.5.2). However Table 3 contains 20 clusters above this threshold, which are not in the list of De Grandi et al. (1999). The reason is that these sources were not in the RASS-1 source list, but were found by the RASS-2 analysis as a consequence of the improvements, in particular lowering source detection thresholds and searching for sources in the hard energy band, which are described in section 3.1 and by Voges et al. (1999). These 20 sources are NGC 720, NGC 1132, five newly discovered clusters, SH518, and the Abell clusters 194, 2410, 2442, 2474, 2496, 2554, 2556, 2566, 3984, 4010, 4068 and S1136. The SGP catalog contains 113 clusters having fluxes below the threshold of the De Grandi et al. (1999) study.

The log N-log S distribution for the SGP cluster sample is shown in Figure 11, where it is compared with the results of other surveys. To avoid any errors caused by converting hard band (0.5 – 2.0 keV) fluxes in these surveys to broad band (0.1 – 2.4 keV) fluxes, we have made this comparison in the hard band. The circular symbols (\circ) are the result of the survey of clusters by De Grandi et al. (1999), who reanalysed clusters detected in the RASS-1 data base over a 2.5 ster area of the southern sky and made first use of redshifts obtained from the ESO Key Project. Figure 11 includes also one point from the HEAO-1 A-2 cluster survey (Piccinotti et al. 1982), the fit to the log N-log S curve obtained by Ebeling et al. (1998) from the ROSAT Brightest Cluster sample (BCS), and a box setting limits at low fluxes, derived from an analysis of EMSS results (Rosati et al. 1995). There are significant differences among these results at energy fluxes less than $1 \times 10^{-11} \text{ erg cm}^{-2} \text{ s}^{-1}$. There is a flattening of the SGP log N-log S distribution at energy fluxes less than about

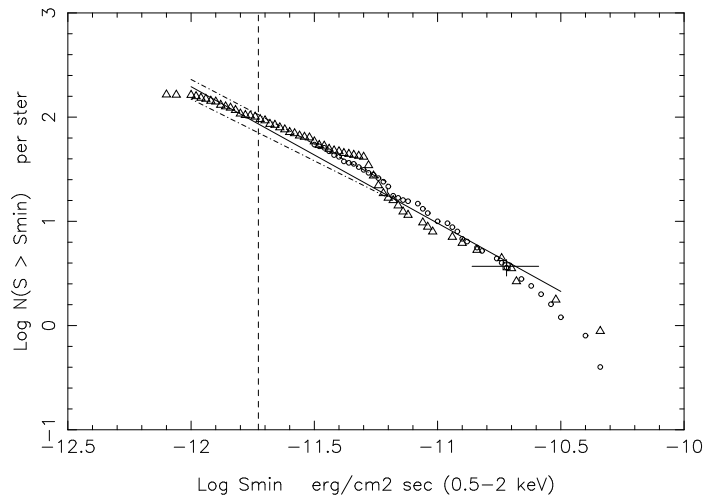


Fig. 11.— The log N-log S distribution of the SGP cluster sample is traced by the symbols \triangle . The distribution obtained by De Grandi et al. (1999) is shown by the symbols \circ . The solid line is the fit of Ebeling et al. (1998) and the dot-dash line shows limits set by Rosati et al. (1995) using the EMSS survey results. The point (\square) with error bars was obtained from Piccinotti et al. (1982). For comparison purposes all fluxes in this plot refer to the energy band 0.5 – 2.0 keV. The vertical dashed line corresponds to a flux limit in the 0.1 – 2.4 keV band of $3 \times 10^{-12} \text{ erg cm}^{-2} \text{ s}^{-1}$.

$1.8 \times 10^{-12} \text{ erg cm}^{-2} \text{ s}^{-1}$, equivalent to a flux of $3 \times 10^{-12} \text{ erg cm}^{-2} \text{ s}^{-1}$ in the ROSAT broad band (0.1 – 2.4 keV), which is the completeness limit derived in section 6. Applying this limit we obtain a sample of 112 clusters, of which 110 have measured redshifts. The sources of the incompleteness of the SGP catalog at low fluxes have been discussed in section 3.5.5.

In addition there is a steepening of the SGP log N-log S curve over a short range of hard band flux near $5 \times 10^{-12} \text{ erg cm}^{-2} \text{ s}^{-1}$, a characteristic evident to a lesser extent also in the results of De Grandi et al. (1999). This results in the distribution being higher than the fit of Ebeling et al. (1998) and being at the upper limit set by Rosati et al. (1995), within the range $3 - 5 \times 10^{-12} \text{ erg cm}^{-2} \text{ s}^{-1}$. This may be a statistical fluctuation, but as we show in section 7, there is significant large-scale structure in the SGP field out to a redshift of $z \sim 0.15$, which may be one cause of this feature in the SGP log N-log S distribution (Figure 11).

The optical observing program and a search of the literature yielded redshifts for 157 of the 186 clusters in Table 3. The distribution of the clusters in redshift space is summarised in the 'wedge' diagram shown in Figure 12, in which the clusters are projected onto a plane whose co-ordinates are cluster redshift and right ascension. In this figure the symbol size is a measure of the cluster X-ray luminosity in the 0.1 – 2.4 keV band.

Table 3 contains five sources, labelled 'dc' in column 11, for which the X-ray and optical data provide compelling evidence that they are interacting double clusters. In contrast the pair of objects RXCJ0108.8-1524 and RXCJ0108.9-1537, which in projection are close, do not constitute a double cluster as they are well separated in redshift space. The former is A151, which has a redshift of 0.0537 (H. Andernach 1989, unpublished, private communication), whereas spectroscopic observation of the latter yield two redshifts which tie the galaxies to A151 but nine having a mean of 0.0981 ± 0.0027 (rms) (Katgert et al. 1996, 1998).

6. TESTS OF SAMPLE COMPLETENESS

In section 3.5.5 it was estimated from a comparison of the number of clusters detected in the SGP with the CSEARCH predictions, that the sample completeness was 0.79, and it was concluded that the missing ones were mainly distant clusters of small angular extent. The effect is to flatten the log N-log S distribution at low fluxes (Figure 11), and using the following arguments we have established that the sample is essentially complete at fluxes greater than $3.0 \times 10^{-12} \text{ erg cm}^{-2} \text{ s}^{-1}$.

First, we compare our log N-log S distribution with the results of deeper surveys, and of the wider field REFLEX and BCS surveys. At $3.0 \times 10^{-12} \text{ erg cm}^{-2} \text{ s}^{-1}$ in the SGP dis-

Table 4. Explanation with appropriate references of the prefixes to the source optical identification, which is given in column 11 of Table 3.

Prefix	Source of Optical Identification	Reference
A	Abell catalog	Abell et al. (1989)
S	Abell catalog: southern supplementary clusters	Abell et al. (1989)
AM	Cambridge APM catalog	NED: Arp & Madore (1987)
APMCC	Cambridge APM cluster catalog	Dalton et al. (1997)
CID	EFAR survey	Barton et al. (1996)
EDCC	Edinburgh-Durham cluster catalog	Lumsden et al. (1992)
EMSS	EINSTEIN medium sensitivity survey	Stocke et al. (1991)
ESO	European Southern Observatory	No reference in NED
HCG	Hickson compact group catalog	Hickson (1982), Barton et al. (1996)
SCG	Catalog of COSMOS southern compact groups	Prandoni, Iovino & MacGillivray (1994)
NGC	Cluster dominated by NGC galaxy	NED
SH	Cluster catalog from Shane-Wirtanen galaxy counts	Shectman (1985)

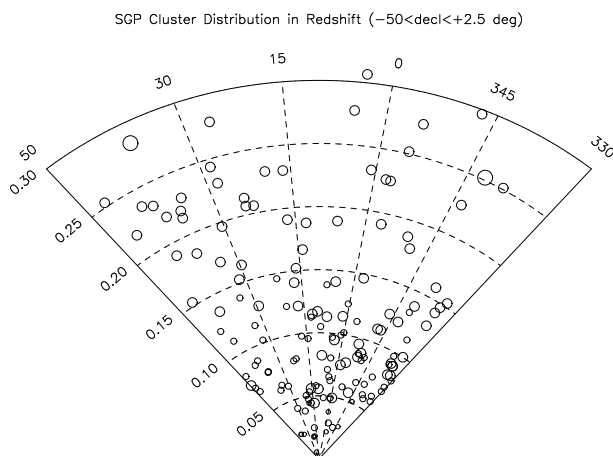


Fig. 12.— A 'wedge' diagram showing the distribution in redshift of all the clusters in the catalog (Table 3), for which measured redshifts are available. The symbol size is a measure of X-ray luminosity in the hard energy band.

tribution (Figure 11) we obtain $N = 100 \pm 9 \text{ ster}^{-1}$. For deeper surveys, which have smaller fields and therefore limited statistics at this flux, we obtain $N = 87 \pm 15 \text{ ster}^{-1}$ (Rosati et al. 1998), $N = 70 \pm 10 \text{ ster}^{-1}$ (Vikhlinen et al. 1998), $N = 125_{-66}^{+98} \text{ ster}^{-1}$ (Henry et al. 2001), and $N = 87_{-38}^{+69} \text{ ster}^{-1}$ (Gioia et al. 2001). For the REFLEX survey we obtain $N = 94 \pm 5 \text{ ster}^{-1}$ (Böhringer et al. 2001) and for the BCS survey $N = 95 \pm 5 \text{ ster}^{-1}$ (Ebeling et al. 1998). We find no evidence that the SGP result is inconsistent with these surveys at this flux threshold.

Second, we apply a standard measure of the formal completeness of a sample, namely the V/V_{max} test (e.g., Schmidt 1968, Avni & Bahcall 1980). For the computation of the maximum volume V_{max} the effective area, the local variation of the X-ray flux limit (both for a minimum of 10 source counts), and the K correction (see section 4) are taken into account. The test is performed for subsamples with different X-ray flux limits. The mean of the V/V_{max} values and their 2σ standard deviations are plotted in Figure 13. Note that the errors do not include cosmic variance. Below $2 \times 10^{-12} \text{ erg cm}^{-2} \text{ s}^{-1}$ the deviations from the ideal value of 0.5 are significant, indicating that the sample gets definitively incomplete below this flux limit. Between 2×10^{-12} and $3.0 \times 10^{-12} \text{ erg cm}^{-2} \text{ s}^{-1}$ it is difficult to make a definite statement about significant deviations from the 0.5 line because the large scale inhomogeneities in the spatial distribution of the clusters (see section 7) start to modulate the averaged V/V_{max} values. Note also that the measurements at different flux limits are not statistically independent. A good estimate of the flux completeness limit is $f_x^{\text{lim}} = 3 \times 10^{-12} \text{ erg cm}^{-2} \text{ s}^{-1}$, because for fluxes brighter than this limit the averaged V/V_{max} values are all within the 90 percent confidence range (note that cosmic variance increase the given formal errors).

Third, we examine the behavior of the radially averaged comoving cluster number density along the redshift direction. If we assume that within the tested redshift range no large evolutionary effects are present, one would expect an almost constant cluster number density profile with superposed large-scale inhomogeneities. Figure 14 shows the superposition of a set of cluster number density profiles obtained from 10 volume-limited subsamples within the luminosity range 5.0×10^{43} to $2.0 \times 10^{45} \text{ erg s}^{-1}$. Outside this luminosity interval the sizes of the subsamples are smaller than 10 and are thus dominated by small-number statistics. The subsamples are restricted to clusters with at least 10 source counts and X-ray fluxes larger than $3.0 \times 10^{-12} \text{ erg cm}^{-2} \text{ s}^{-1}$, as obtained from the V/V_{max} test mentioned above. The effective survey area covered by each subsample is taken into account. The individual density profiles are normalized using the average cluster number density estimated for each subsample. The bars in Figure 14 represent the formal 1σ Poisson errors, within which no systematic large-scale gradients of the number density are found for $z \leq 0.25$. The comparatively large high-density region found in the redshift interval $0.05 - 0.10$ is composed mainly of several superclusters. A more detailed analysis of the large-scale structure is given

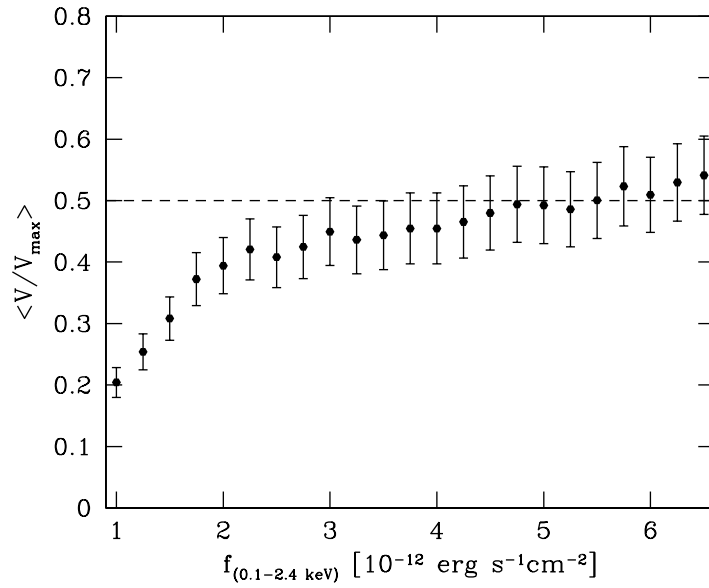


Fig. 13.— Mean V/V_{max} values as a function of flux limit. The error bars are the formal 2σ Poisson errors. The dashed line corresponds to the ideal case of a complete sample. It is seen that below $3.0 \times 10^{-12} \text{ erg cm}^{-2} \text{ s}^{-1}$ the sample becomes incomplete.

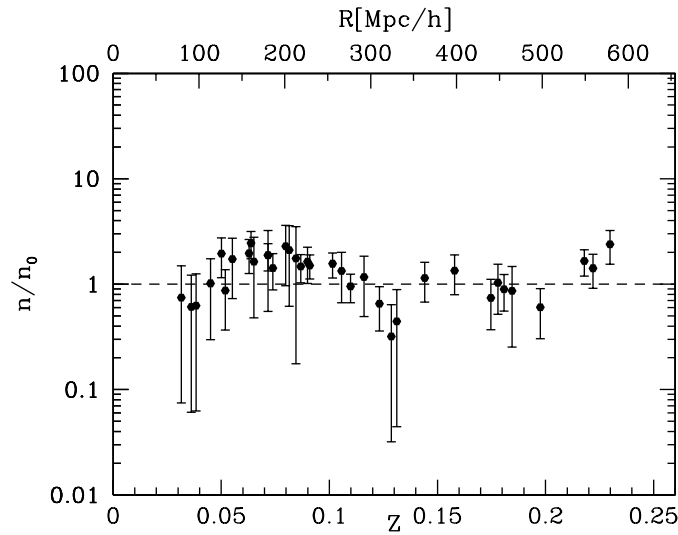


Fig. 14.— Comoving cluster number densities as a function of redshift obtained from 10 subsamples covering the luminosity range from 5.0×10^{43} to 2.0×10^{45} erg s⁻¹. The clusters have fluxes larger than 3.0×10^{-12} erg cm⁻² s⁻¹ and at least 10 source counts. No indications for systematic large-scale density gradients are seen, suggesting the absence of strong incompleteness effects.

in section 7.

Finally, we have verified that the variation of RASS exposure time in the SGP field (Figure 1) has little effect on the effective area at a flux level of $3.0 \times 10^{-12} \text{ erg cm}^{-2} \text{ s}^{-1}$. At the detection threshold of the GCA (10 source counts), this area is 98 percent of the total area of the field.

7. LARGE-SCALE STRUCTURE IN THE SGP REGION

The 'wedge' diagram for the SGP cluster sample (Figure 12) reveals that the spatial density of clusters at redshifts greater than 0.15 is too low for the purpose of tracing large-scale structure, and we concentrate the discussion on clusters within this limit. A detailed examination of large-scale structure in the southern sky was made by Tully et al. (1992), who analysed the Abell, Corwin & Olowin (1989) catalog of clusters. In this study measured redshifts were complemented by estimates based on the magnitudes of the third and tenth brightest galaxies, having an accuracy of $\pm 22\%$ (rms) out to redshifts of about 0.2 (Zamorani et al. 1992). We have condensed the results into a sky map of the centroids of superclusters identified in the SGP region (Figure 15). Another 'wedge' diagram (Figure 16) shows the distribution of these superclusters in redshift space.

The dotted line in Figure 15 traces the supergalactic equator, defined by the plane of a 'disk-like' structure, the Local Supercluster, identified by De Vaucouleurs & De Vaucouleurs (1964) using measurements of the radial velocities of a large sample of local galaxies. The maximum values of these velocities were around 10000 km s^{-1} ($z \simeq 0.03$). Tully et al. (1992) have presented persuasive evidence that the Pisces-Cetus supercluster is likewise a flattened structure extending along the supergalactic equator, which is an extension of the Local Supercluster out to redshifts of at least 0.06. This idea is supported by our X-ray survey of clusters in the SGP. Figure 17 is a sky map of all clusters in the SGP catalog (Table 3) having a redshift of less than 0.075, which shows clearly a concentration of clusters around the supergalactic equator (Figure 15). Of the 36 clusters identified by Tully (1987) as members of the Pisces-Cetus supercluster, the following seven appear in Table 3 and have a redshift $z < 0.075$: A14, A85, A119, A133, A147, A151, and A168. The six brightest clusters in Figure 17, having hard-band X-ray count rates greater than 0.9 ct s^{-1} , lie close to the supergalactic equator. Five of these clusters, A85, A119, A133, A4059 and S1101, have redshifts between 0.0444 and 0.0564, consistent with their being members of the Pisces-Cetus supercluster. The fifth, A4038, is nearer at a redshift of 0.0283, placing it at the edge of the Local Supercluster. The Pisces-Cetus supercluster is evident also in the 'wedge' diagram (Figure 12), in which the group of X-ray clusters at R.A. $\sim 15^\circ$ and $z \sim 0.05$ is close to the

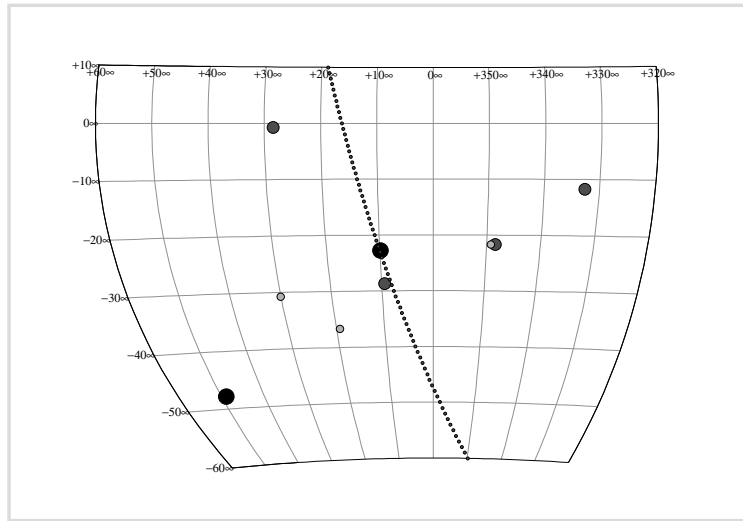


Fig. 15.— The map shows the locations of the centroids of superclusters (SC) identified in Tully et al. (1992) in the SGP region. The symbol size is a rough measure of distance, decreasing as redshift increases. The following notes identify the superclusters and the centroid positions: Pisces-Cetus (10,-23), Horologium-Reticulum (49,-48), Sculptor A (9,-29), Aquarius A (348,-22), Aquarius B (349,-22), Aquarius-Capricornus (333,-12), Cetus (28,-1), Fornax (30,-31) and Sculptor B (19,-37). The dotted line traces the supergalactic equator

location of the supercluster center.

More distant structures are difficult to identify in the X-ray survey. Tully et al. (1992) identified a structure orthogonal to the supergalactic equator, which includes the superclusters Aquarius A and B, Aquarius-Capricornus, and Sculptor A and B. The location of this structure, which extends from $z \sim 0.05$ to $z \sim 0.12$ ($\sim 130 - 330h^{-1}$ Mpc), may be traced in Figures 15 and 16. To search for evidence of this structure in the X-ray data, we have constructed a sky map (Figure 18) which includes only X-ray clusters in the range $0.075 < z < 0.125$. The map shows an elongated feature in the NW quadrant, which is perpendicular to the supergalactic equator. The argument that this feature traces the structure evident in the findings of Tully et al. (1992) is supported by two observations. First, the group of X-ray clusters in the NW corner of Figure 18 belongs to the Aquarius-Capricornus supercluster. A correlation in sky position is evident upon comparing Figures 18 and 15, and a correlation in redshift space is seen upon comparing Figures 12 and 16. Second, the two bright clusters A2597 and A2670, highlighted as black circles in the NW quadrant, were identified by Tully (1987) as members of the Aquarius supercluster.

Batuski et al. (1999) have performed redshift measurements recently which establish that Aquarius A and B are essentially one filamentary structure almost aligned with the line-of-sight between $z = 0.08$ and $z = 0.15$. This concentration of Abell clusters on the sky near $\alpha = 350^\circ$, $\delta = -22^\circ$ (Batuski et al. 1999) is not evident in the X-ray data (Figure 18). However, care is needed in interpreting this result as it may be biased by the relatively low exposure time in this part of the RASS (Figure 1).

Therefore we conclude that, at least for redshifts out to $z \sim 0.15$, there is significant large-scale structure in the SGP field. However, there is one part of this structure which is not strongly evident in the X-ray maps shown in Figure 17 and Figure 18. This is the Horologium-Reticulum supercluster (Tully et al. 1992), a rich association of clusters having its centroid at $z = 0.063$ and located at the position shown in Figure 15. There is only one bright X-ray cluster in our survey, A3113 at $(49.49, -44.24)$, Figure 18) and $z = 0.0754$, which may be associated with this supercluster. We cannot rule out the possibility that the supercluster is inconspicuous because of its location close to the boundary of the SGP survey region.

8. SUMMARY AND CONCLUSIONS

A systematic search of the ROSAT all-sky survey for clusters of galaxies has been performed in an area of 1.013 ster centered on the South Galactic Pole. The search was made

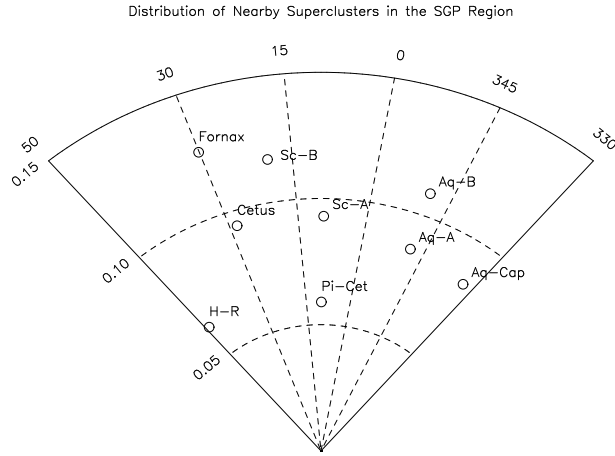


Fig. 16.— A 'wedge' diagram showing the distribution in redshift space of the supercluster centroids shown in Figure 15. The labels identify the superclusters.

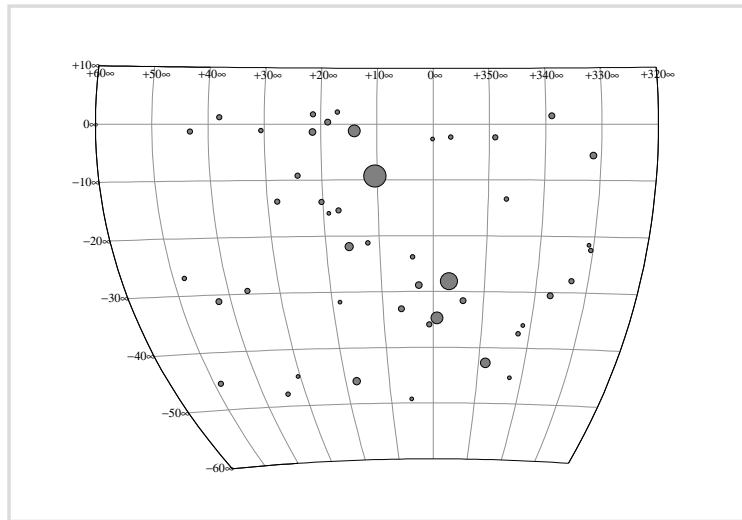


Fig. 17.— A sky map of clusters of galaxies detected by the ROSAT sky survey in a region centered on the south galactic pole and having an area of 1.013 ster. The map shows only clusters having a redshift $z < 0.075$. The symbol size is a measure of the X-ray count-rate in the hard energy band (0.5 – 2 keV).

by correlating the list of RASS sources detected in the hard X-ray band (0.5 – 2.0 keV) with the projected surface density of galaxies derived from the COSMOS digitised UK Schmidt IIIa-J survey of the southern sky. The analysis yielded a list of 3236 candidates, of which ~ 50 percent should be chance associations with non-cluster sources, mainly AGN and stars, and which should be 90 percent complete in containing clusters. The study was bounded during X-ray analysis by applying a lower limit of 0.08 ct s^{-1} to the count-rate in the hard band, yielding a list of 477 candidates.

Non-cluster sources were removed by applying tests using the source X-ray extent and hardness ratio, by scrutiny of COSMOS finding charts and overlays of the RASS and COSMOS images, and by correlation with such catalogs as the NASA Extragalactic (NED), SIMBAD, TYCHO and Veron data bases. This was performed in as objective a manner as possible, requiring an iterative sequence of procedures. The search resulted in 186 clusters, comprising 134 Abell clusters, 15 clusters found in other catalogs, and 37 newly discovered clusters. The catalog shown in Table 3, and the overlays of the RASS hard X-ray and COSMOS optical images, are accessible over the Internet (<http://wave.xray.mpe.mpg.de/publications/papers/2001/RSGP-clusters/xray-optical-images>). The catalog has a minimum energy flux of $\sim 1.5 \times 10^{-12} \text{ erg cm}^{-2} \text{ s}^{-1}$ in the band 0.1 – 2.4 keV. Tests show that a sample of 112 clusters, obtained when a flux limit of $3.0 \times 10^{-12} \text{ erg cm}^{-2} \text{ s}^{-1}$ is applied, is essentially complete. We estimate the completeness of the overall catalog at a flux limit of $1.5 \times 10^{-12} \text{ erg cm}^{-2} \text{ s}^{-1}$ to be ≤ 80 percent.

In support of studies of cluster evolution and large-scale structure using the results of the survey, a series of optical observing campaigns at the AAT and at SAAO was conducted to obtain cluster redshifts. In addition we have used a number of redshifts obtained in programs at ESO in support of the REFLEX project. Using these campaigns and an extensive search of the literature we have obtained redshifts for 157 of the clusters in the catalog (Table 3). Redshifts are available for 110 of the 112 clusters in the complete flux-limited sample.

Examination of the spatial distribution of the SGP X-ray cluster sample corroborates earlier studies of large-scale structure, which were based on optical observations (De Vaucouleurs & De Vaucouleurs 1964, Tully et al. 1992). The basic features are a flattened structure in the supergalactic plane, reaching out to $z \sim 0.07$ and embracing the Pisces-Cetus supercluster, and an orthogonal structure at $0.07 < z < 0.15$ which includes the Aquarius, Aquarius-Capricornus and Sculptor A and B superclusters.

We thank Prof. Trümper and the ROSAT team for the unstinting support, the myriad valuable discussions, the access to the RASS data base, the use of the RASS and EXSAS software, and the use of the powerful computing system under Joachim Paul and his team,

which have made this work possible. The ROSAT Project is supported by the Bildungsministerium für Bildung und Forschung (BMBF/DLR) and the Max-Planck-Gesellschaft (MPG). In equal measure we thank the Royal Observatory Edinburgh and the Naval Research Laboratory (NRL) for the intensive effort that went into the creation of the COSMOS digitised optical data base and its installation at MPE, which was an essential factor in identifying clusters in the RASS data base. Our gratitude goes also to the Anglo-Australian Telescope, the South African Astronomical Observatory and the European Southern Observatory for the expert assistance provided to the optical observations crucial to this project. We thank the REFLEX project for its cooperation in exchanging redshifts, and in particular Luigi Guzzo of the Osservatorio Astronomica di Brera for his analysis of those ESO Key Project observations, which yielded 14 redshifts used in this study. Finally, this research has been supported by the Office of Naval Research and NRL, and by the National Aeronautics and Space Administration through an Astrophysics Data Program grant (S57759-F).

REFERENCES

- Abell, G. O., Corwin Jr., H. G., & Olowin, R. P. 1989, *ApJS*, 70, 1
- Arp, H. C., & Madore, B. F. 1987, "A Catalogue of Peculiar Galaxies and Associations (Cambridge: Cambridge University Press)
- Avni, Y. & Bahcall, J.N. 1980, *ApJ*, 235, 694
- Barton, E., Geller, M. J., Ramella, M., Marzke, R. O., & Da Costa, L. N. 1996, *AJ*, 112, 871
- Batuski, D. J., Miller, C. J., Slingsend, K. A., Balkowski, C., Maurogordato, S., Cayatte, V., Felenbok, P., & Olowin, R. 1999, *ApJ*, 520, 491
- Böhringer, H., et al. 2000, *ApJS*, 129, 435
- Böhringer, H., et al. 2001, *A&A*, 369, 826
- Caretta, C. A., Maia, M. A. G., & Willmer, C. N. A. 2000, *AJ*, 119, 524
- Cavaliere, A., & Fusco-Femiano, R. 1976, *A&A*, 49, 137
- Collins, C. A., Guzzo, L., Nichol, R. C., & Lumsden, S L. 1995, *MNRAS*, 274, 1071
- Collins, C. A., Burke, D. A., Romer, A.K., Sharples, R. M., & Nichol, R. C. 1997, *ApJ*, 479, L117
- Collins, C. A., et al. 2000, *MNRAS*, 319, 939
- Crawford, C. S., Edge A. C., Fabian, A. C., Allen, S. W., Boehringer, H., Ebeling, H., McMahon, R. G. & Voges, W. 1995, *MNRAS*, 274, 75
- Da Costa, L. N., et al. 1998, *AJ*, 116, 1
- Dalton, G. B., Efstathiou, G. & Sutherland, W. J. 1994, *MNRAS*, 269, 151
- Dalton, G. B., Maddox, S. J., Sutherland, W. J., & Efstathiou, G. 1997, *MNRAS*, 289, 263

- De Grandi, S., Molendi, S., Böhringer, H., & Voges, W. 1997, *ApJ*, 486, 738
- De Grandi, S., et al. 1999, *ApJ*, 514, 148
- De Vaucouleurs, G., & De Vaucouleurs, A. 1964, *First Reference Catalogue of Bright Galaxies* (Austin, University of Texas Press)
- De Vaucouleurs, G., De Vaucouleurs, A., Corwin, H., Buta, R., Paturel, G. & Fouque, P. 1991, *Third Reference Catalogue of Bright Galaxies* (Springer-Verlag: New York)
- Di Nella, H., Couch, W. J., Paturel, G., & Parker, Q. A. 1996, *MNRAS*, 283, 367
- Dickey, J. M., & Lockman, F. J. 1990, *Ann. Rev. Astron. Astrophys.*, 28, 215
- Ebeling, H., & Wiedemann, G. 1993, *Phys. Rev. E*, 47, 704
- Ebeling, H., & Maddox, S. J. 1995, *MNRAS*, 275, 1155
- Ebeling, H., Voges, W., Böhringer, H., Edge, A. C., Huchra, J. P., & Briel, U. G. 1996, *MNRAS*, 281, 799
- Ebeling, H., Edge, A. C., Böhringer, H., Allen, S. W., Crawford, C. S., Fabian, A. C., Voges, W., & Huchra, J. P. 1998, *MNRAS*, 301, 881
- Ebeling, H., Edge, A. C., Allen, S. W., Crawford, C. S., Fabian, A. C., & Huchra, J. R. 2000, *MNRAS*, 318, 333
- Edge, A. C., Stewart, G. C., Fabian, A. C., & Arnaud, K. A. 1990, *MNRAS*, 245, 559
- Fetisova, T. S., Kuznetsov, D. Yu., Lipovetski, V. A., Starobinski, A. A., & Olovin, R. P. 1993, *Astronomy Letters*, 19, 198
- Gioia, I. M., Henry, J. P., Mullis, C. R., Voges, W., Briel, U. G., Böhringer, H. & Huchra, J. P. 2001, *ApJ*, 553, L105
- Henry, J.P., Gioia, I. M., Maccacaro, T., Morris, S. L., Stocke, J. T., & Wolter, A. 1992, *ApJ*, 386, 408
- Henry, J. P., Gioia, I. M., Mullis, C. R., Voges, W., Briel, U. G., Böhringer, H. & Huchra, J. P. 2001, *ApJ*, 553, L109
- Heydon-Dumbleton, N. H., Collins, C. A., & MacGillivray, H. T. 1989, *MNRAS*, 238, 379
- Hickson, P. 1982, *ApJ*, 255, 382
- Høg, E., Kuzmin, A., Bastian, U., Fabricius, C., Kuimov, K., Lindegren, L., Makarov, V. V., & Röser, S. 1998, *A&A*, 335, L65
- Huchra, J. P., Vogeley, M. S. & Geller, M. J. 1999, *ApJS*. 121, 287
- Katgert, P., et al. 1996, *A&A*, 310, 8
- Katgert, P., Mazure, A., den Hartog, R., Adami, C., Biviano, A., & Perea, J. 1998, *A&AS*, 129, 399
- Kowalski, M. P., Ulmer, M. P., Cruddace, R. G., & Wood, K. S. 1984, *ApJS*, 286, 822
- Jones, L. R., Scharf, C., Ebeling, H., Perlman, E., Wegner, G., Malkan, M., & Horner, D. 1998, *ApJ*, 495, 100
- Lauberts, A., & Valentijn, E. 1989, *ESO catalog, "The Surface Photometry of the ESO-Uppsala Galaxies"* (European Southern Observatory: Garching)

- Lumsden, S. L., Nichol, R. C., Collins, C. A., & Guzzo, L. 1992, MNRAS, 258, 1
- MacGillivray, H. T., & Stobie, R. S. 1985, *Vistas in Astronomy*, 27, 433
- Mazure, A., et al. 1996, A&A, 310, 31
- McHardy, I. 1978, MNRAS, 184, 783
- Mullis, C.R., Henry, J. P., Gioia, I. M., Böhringer, H., Briel, U. G., Voges, W. & Huchra, J. P. 2000, ApJ, 553, L115
- Muriel, H., Nicotra, M. A., & Lambas, D. G. 1995, AJ, 110, 1032
- Piccinotti, G., Mushotzky, R. F., Boldt, E. A., Holt, S. S., Marshall, F. E., Serlemitsos, P. J., & Shafer, R. A. 1982, ApJ, 253, 485
- Postman, M., Huchra, J. P., & Geller, M. J. 1992, ApJ, 384, 404
- Prandoni, I., Iovino, A., & MacGillivray, H. T. 1994, AJ, 107, 1235
- Quintana, H., & Ramirez, A. 1995, ApJS, 96, 343
- Ratcliffe, A., Shanks, T., Parker, Q. A., Broadbent, A., Watson, F. G., Oates, A. P., Collins, C. A., & Fong, R. 1998, MNRAS, 300, 417
- Raymond, J. C., & Smith, B. W. 1977, ApJS, 35, 419
- Romer, A. K., Collins, C. A., Böhringer, H., Cruddace, R. G., Ebeling, H., MacGillivray, H. T., & Voges, W. 1994, Nature, 372, 75
- Romer, A. K. 1995, Doctoral Thesis, University of Edinburgh
- Romer, A. K., et al. 2000, ApJS, 126, 209
- Rosati, P., Della Ceca, R., Burg, R., Norman, C., & Giacconi, R. 1995, ApJ, 445, L11
- Rosati, P., Della Ceca, R., Norman, C., & Giacconi, R. 1998, ApJ, 492, L21
- Schmidt, M. 1968, ApJ, 151, 393
- Schwartz, D. A. 1978, ApJ, 220, 8
- Shectman, S. A. 1985, ApJS, 57, 77
- Shectman, S. A., Landy, S. D., Oemler, A., Tucker, D. L., Lin, H., Kirschner, R. P., & Schechter, L. P. 1996, ApJ, 470, 172
- Schuecker, P., et al. 2001, A&A, 368, 86
- Stoche, J. T., Morris, S. M., Gioia, I. M., Maccacaro, T., Schild, R., Wolter, A., Fleming, T. A., & Henry, J.P. 1991, ApJS, 76, 813
- Struble, M. F., & Rood, H. J. 1999, ApJS, 125, 35
- Trümper, J. 1983, Adv. Space Res., 27, 1404
- Trümper, J., et al. 1991, Nature, 349, 579
- Tucker, W. H., Tananbaum, H., & Remillard, R. A. 1995, ApJ, 444, 532
- Tully, R. B. 1987, ApJ, 323, 1
- Tully, R. B., Scaramella, R., Vettolani, G., & Zamorani, G. 1992, ApJ, 388, 9
- Veron-Cetty, M. P., & Veron, P. 1998, ESO Scientific Report 18
- Vikhlinen, A., McNamara, B. R., Forman, W., & Jones, C. 1998, ApJ, 502, 558
- Voges, W., et al. 1999, A&A, 349, 389

- Voges, W., et al. 2000, IAU Circular 7432
- Voges, W., Henry, J. P, Briel, U. G., Böhringer, H., Mullis, C. R., Gioia, I. M. & Huchra, J. P. 2001, ApJ, 553, L119
- White, D. A., Jones, C., & Forman, W. 1997, MNRAS, 292, 419
- Yentis, D. J., Cruddace, R. G., Gursky, H., Stuart, B. V., Wallin, J. F., MacGillivray, H. T., & Collins, C. A. 1992, "Digitised Optical Sky Surveys", ed. H. T. MacGillivray & E. B. Thomson, (Netherlands: Kluwer Academic Publishers), 67
- Zamorani, G., Scaramella, R., Vettolani, G., & Chincarini, G. 1992, in "Traces of Primordial Structure in the Universe", ed. H. Böhringer & R. A. Tremann, MPE Report 227

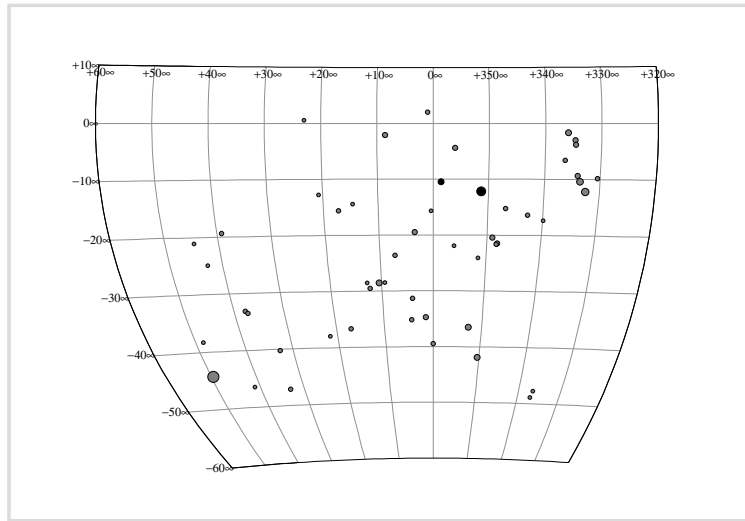


Fig. 18.— A sky map of those clusters in the ROSAT SGP sample, which have redshifts in the range $0.075 < z < 0.125$. The two black circles in the NW quadrant are A2597 and A2670, identified by Tully (1987) as members of the Aquarius supercluster association.

Table 3. Catalog of clusters in the SGP

Source (1)	RA (J2000) (2)	Decl (J2000) (3)	Count rate (4)	HR (5)	Time N_H (6)	T_x (7)	f_x (8)	L_x (9)	Identification (10)	Redshift (11)	Ref(z) (12)	N_g (13)	N_g (14)
RXCJ2201.8-2226	22 01 50.5	-22 26 37	0.286±0.043	0.82±0.30	237	2.61	3.554 ^e	5.75	1.193	S987	0.0693	8	20
RXCJ2202.1-0949	22 02 07.2	-09 49 48	0.280±0.038	1.15±0.31	307	4.20	4.039 ^e	5.89	1.629	A2410	0.0801	17	1
RXCJ2203.8-2130	22 03 50.6	-21 30 31	0.139±0.030	0.11±0.19	227	2.45	2.809 ^e	2.77	0.644		0.0732	1	3
RXCJ2205.6-0535	22 05 39.6	-05 35 29	0.674±0.109	0.79±0.12	191	4.68	3.800	14.40	2.103	A2415	0.0582	2	3
RXCJ2210.3-1210	22 10 20.0	-12 10 33	0.746±0.056	1.04±0.08	278	3.92	6.000	15.70	4.642	A2420	0.0831	1	3
RXCJ2213.0-2753	22 13 05.0	-27 53 56	0.425±0.034	0.14±0.17	205	1.40	3.760 ^e	8.28	1.373		0.0620	1	2
RXCJ2214.4-1701	22 14 26.3	-17 01 24	0.198±0.020	0.79±0.24	305	2.61	5.845 ^e	4.02	4.016	A3847	0.1530	3	1
RXCJ2214.5-1022	22 14 32.4	-10 22 12	0.594±0.052	0.95±0.09	280	3.84	6.578 ^e	12.50	5.343	A2426	0.1001	1	4
RXCJ2216.2-0920	22 16 15.2	-09 20 18	0.405±0.041	0.87±0.09	274	5.24	4.869 ^e	8.78	2.567	A2428	0.0825	1	2
RXCJ2216.9-1725	22 16 56.4	-17 25 30	0.425±0.034	0.35±0.12	277	2.28	6.969 ^e	8.56	6.163		0.1301	1	2
RXCJ2217.7-3543	22 17 43.7	-35 43 32	0.329±0.035	0.32±0.11	319	1.10	6.865 ^e	6.42	5.929	A3854	0.1474	13	9
RXCJ2218.2-0350	22 18 17.1	-03 50 01	0.427±0.047	0.92±0.14	273	5.73	5.375 ^e	9.39	3.267	MS2215.7-0404 dc	0.0901	1	3
RXCJ2218.6-3853	22 18 40.3	-38 53 48	0.425±0.034	0.27±0.09	314	1.33	7.246 ^e	8.35	6.746	ESO 344-G 019	0.1379	28	?
RXCJ2218.8-0258	22 18 49.0	-02 58 07	0.425±0.034	0.90±0.19	268	5.84	5.350 ^e	9.37	3.246		0.0899	2	7
RXCJ2223.9-0137	22 23 56.7	-01 37 44	0.454±0.049	1.00±0.12	224	5.34	9.000	9.92	3.509	A2440	0.0912	8	24
RXCJ2225.8-0636	22 25 50.8	-06 36 09	0.239±0.034	0.68±0.15	251	5.14	4.196 ^e	5.16	1.787	A2442	0.0897	2	12
RXCJ2226.1-4745	22 26 10.6	-47 45 01	0.091±0.020	0.31±0.23	329	1.44	3.289 ^e	1.77	0.978	A3876	0.1130	14	?
RXCJ2227.4-4852	22 27 28.3	-48 52 54	0.126±0.022	0.24±0.17	367	1.65	3.321 ^e	2.47	1.004	APMCC782	0.0970	14	3
RXCJ2227.8-3034	22 27 52.9	-30 34 11	0.522±0.043	0.05±0.06	308	1.09	3.800	10.10	1.415	A3880	0.0570	13	11
RXCJ2231.2-3802	22 31 15.1	-38 02 39	0.088±0.022	0.88±0.44	233	1.20	5.000 ^e	1.71					
RXCJ2234.5-3744	22 34 30.4	-37 44 05	0.573±0.051	0.09±0.07	241	1.22	7.900	11.20	11.986	A3888	0.1590	8	70
RXCJ2234.8-3033	22 34 53.5	-30 33 56	0.119±0.027	0.64±0.28	305	1.11	6.983 ^e	2.32	6.182	A3889	0.2512	8	19
RXCJ2235.6+0128	22 35 40.6	+01 28 21	0.510±0.080	0.76±0.12	167	5.81	4.113 ^e	11.20	1.702	A2457	0.0594	3	18
RXCJ2239.2-1719	22 39 16.4	-17 19 46	0.102±0.033	0.76±0.33	110	2.99	2.559 ^e	2.05	0.503	A2462	0.0751	17	1
RXCJ2241.9-4235	22 41 56.7	-42 35 51	0.085±0.022	0.49±0.25	259	1.66	5.000 ^e	1.68		A3902	0.1500	1	6
RXCJ2243.0-2010	22 43 05.1	-20 10 34	0.246±0.098	0.71±0.20	185	2.60	5.892 ^e	4.99	4.085	A2474	0.1385	1	1
RXCJ2244.5-1744	22 44 34.9	-17 44 21	0.128±0.035	0.38±0.29	151	2.79	4.361 ^e	2.60	1.963	A2478	0.1325	1	2
RXCJ2246.1-3600	22 46 11.8	-36 00 22	0.100±0.022	0.40±0.25	260	1.14	2.290 ^e	1.90	0.374		0.0673	1	2
RXCJ2247.2+0204	22 47 15.2	+02 04 35	0.168±0.064	0.93±0.18	151	5.84	5.000 ^e	3.70					
RXCJ2248.7-4431	22 48 43.4	-44 31 41	0.431±0.047	0.47±0.10	208	1.79	11.946 ^e	8.59	22.736	S1063	0.2520	7	?
RXCJ2249.2-3727	22 49 17.6	-37 27 26	0.154±0.028	0.23±0.20	253	1.13	1.388 ^e	2.66	0.096	S1065	0.0289	23	2
RXCJ2250.8-4521	22 50 48.9	-45 21 33	0.104±0.026	0.44±0.30	203	1.88	1.898 ^e	1.99	0.226	S1067	0.0511	21,22	6
RXCJ2251.0-1624	22 51 00.4	-16 24 21	0.255±0.052	0.83±0.16	103	3.16	5.426 ^e	5.24	3.342	A2496	0.1221	1	3
RXCJ2253.5-3343	22 53 34.2	-33 43 21	0.155±0.029	0.29±0.16	195	1.24	7.133 ^e	3.04	6.504	A3934	0.2250	8	6
RXCJ2305.5-4513	23 05 34.7	-45 13 11	0.220±0.094	0.11±0.20	159	1.69	5.132 ^e	4.34	2.919	A3970	0.1253	1	3
RXCJ2306.8-1324	23 06 51.7	-13 24 59	0.200±0.043	0.51±0.24	139	3.07	5.000 ^e	4.10	0.765		0.0659	2	2
RXCJ2307.2-1513	23 07 15.5	-15 13 41	0.242±0.063	1.12±0.12	90	2.78	4.894 ^e	4.92	2.599	A2533	0.1110	5	1
RXCJ2308.3-0211	23 08 23.1	-02 11 32	0.200±0.029	1.11±0.22	354	4.29	10.221 ^e	4.26	15.544	A2537	0.2966	1	2
RXCJ2312.2-2129	23 12 16.3	-21 29 35	0.335±0.051	0.63±0.20	86	2.03	4.100	6.65	3.532	A2554	0.1111	3	28
RXCJ2313.0-2138	23 13 02.2	-21 38 07	0.273±0.070	0.41±0.15	88	2.03	4.700	5.43	1.746	A2556	0.0865	3	2
RXCJ2313.9-4243	23 13 58.2	-42 43 59	1.185±0.085	0.20±0.06	183	1.85	5.337 ^e	23.50	3.211	S1101	0.0564	1	4
RXCJ2315.7-3746	23 15 44.2	-37 46 53	0.295±0.060	0.54±0.17	128	1.50	7.709 ^e	5.82	7.852	AM 2312-380/A3984	0.1786	1	3
RXCJ2315.7-0222	23 15 46.0	-02 22 38	0.425±0.034	0.80±0.18	337	4.18	2.024 ^e	8.73	0.268	NGC 7556	0.0267	1	2
RXCJ2316.1-2027	23 16 08.0	-20 27 19	0.373±0.068	0.48±0.15	95	2.07	4.589 ^e	7.43	2.222	A2566	0.0834	1	2
RXCJ2321.4-2312	23 21 25.9	-23 12 31	0.164±0.042	0.42±0.21	98	1.96	5.100	3.26	4.883	A2580	0.1870	16	1
RXCJ2321.5-4154	23 21 33.0	-41 54 04	0.440±0.059	0.40±0.12	143	2.15	5.178 ^e	8.80	2.983	A3998	0.0889	1	2
RXCJ2325.3-1207	23 25 20.1	-12 07 40	1.016±0.059	0.44±0.05	322	2.50	9.100	20.60	6.365	A2597	0.0852	8	3
RXCJ2326.2-2406	23 26 16.0	-24 06 13	0.105±0.023	0.73±0.26	185	1.82	2.888 ^e	2.06	0.692	APMCC895	0.0880	14	?
RXCJ2331.1-3630	23 31 11.3	-36 30 22	0.562±0.124	0.54±0.17	51	1.44	6.005 ^e	11.00	4.279	A4010	0.0954	8	8
RXCJ2336.2-3135	23 36 14.9	-31 35 55	0.448±0.057	0.16±0.19	125	1.18	3.712 ^e	8.67	1.320	S1136	0.0594	26,27	2
RXCJ2337.6+0016	23 37 40.9	+00 16 34	0.169±0.033	0.55±0.15	378	3.85	8.948 ^e	3.56	11.264	A2631	0.2753	6	1
RXCJ2338.2-4944	23 38 12.7	-49 44 43	0.094±0.024	0.75±0.28	175	1.89	5.000 ^e	1.87					
RXCJ2341.2-0901	23 41 17.3	-09 01 34	0.168±0.044	0.95±0.16	346	2.55	8.182 ^e	3.41	9.067	A2645	0.2517	8	5
RXCJ2344.2-0422	23 44 16.2	-04 22 07	0.425±0.034	0.69±0.07	335	3.54	4.691 ^e	8.81	2.340		0.0786	1	2
RXCJ2344.4-2153	23 44 28.9	-21 53 34	0.115±0.028	0.61±0.23	198	1.88	3.603 ^e	2.27	1.234	A2655	0.1122	1	3
RXCJ2346.7-1028	23 46 42.4	-10 28 11	0.129±0.024	0.38±0.20	340	2.78	5.872 ^e	2.63	4.093	A2661	0.1911	3	2
RXCJ2347.4-0218	23 47 24.5	-02 18 49	0.180±0.070	1.22±0.23	343	3.62	1.197 ^e	3.08	0.065	HCG 97	0.0221	1	2
RXCJ2347.7-2808	23 47 43.2	-28 08 32	2.546±0.097	0.35±0.03	310	1.55	4.250 ^e	49.90	1.843	A4038	0.0293	8	44
RXCJ2348.2-2849	23 48 13.0	-28 49 01	0.103±0.021	0.09±0.16	309	1.45	6.077 ^e	2.03	4.408	A4041/S1151 dc	0.2260	18	?
RXCJ2350.1-0339	23 50 09.1	-03 39 10	0.125±0.026	1.00±0.23	340	3.65	4.733 ^e	2.60	2.399	A2664	0.1466	6	2
RXCJ2351.6-2605	23 51 40.5	-26 05 09	0.468±0.047	0.48±0.07	308	1.66	11.318 ^e	9.29	19.901	A2667	0.2264	1	1
RXCJ2354.2-1024	23 54 13.5	-10 24 53	0.473±0.057	0.68±0.08	310	2.92	3.900	9.62	2.403	A2670	0.0761	8	220
RXCJ2355.1-2834	23 55 08.6	-28 34 27	0.082±0.020	-0.09±0.16	300	1.49	5.000 ^e	1.61		A4054			
RXCJ2356.0-0129	23 56 02.4	-01 29 43	0.160±0.028	-0.1±0.13	367	3.58	5.000 ^e	3.32					
RXCJ2357.0-3445	23 57 02.4	-34 45 45	1.688±0.093	0.30±0.05	255	1.10	3.500	32.60	3.404	A4059	0.0492	1	2
RXCJ2359.9-3928	23 59 56.8	-39 28 53	0.258±0.047	0.56±0.20	152	1.33	4.595 ^e	5.03	2.229	A4068	0.1016	8	2

Table 3—Continued

Source (1)	RA (J2000) (2)	Decl (J2000) (3)	Count rate (4)	HR (5)	Time (6)	N_H (7)	T_x (8)	f_x (9)	L_x (10)	Identification (11)	Redshift (12)	Ref(z) (13)	N_g (14)
RXCJ0000.4-0237	00 00 24.7	-02 37 30	0.092±0.019	1.00±0.37	372	3.56	1.460 ^e	1.77	0.110		0.0379	24	1
RXCJ0001.6-1540	00 01 39.0	-15 40 52	0.116±0.021	1.00±0.27	337	2.24	3.960 ^e	2.32	1.552		0.1246	1	3
RXCJ0003.1-3555	00 03 11.1	-35 55 21	0.400±0.071	0.29±0.14	142	1.11	3.046 ^e	7.70	0.799	A2717	0.0490	3	56
RXCJ0003.2-0605	00 03 12.0	-06 05 12	0.218±0.027	0.71±0.14	350	3.16	8.577 ^e	4.50	10.167	A2697	0.2320	2	?
RXCJ0003.8+0203	00 03 50.9	+02 03 45	0.205±0.039	0.83±0.12	362	3.00	4.185 ^e	4.18	1.776	A2700	0.0994	1	2
RXCJ0006.0-3443	00 06 04.8	-34 43 26	0.301±0.041	0.23±0.13	226	1.16	5.381 ^e	5.86	3.276	A2721	0.1143	8	72
RXCJ0007.4-2809	00 07 25.3	-28 09 21	0.103±0.022	0.43±0.27	313	1.77	5.000 ^e	2.04		A2726			
RXCJ0011.3-2851	00 11 19.5	-28 51 41	0.612±0.055	0.39±0.09	254	1.84	4.426 ^e	12.10	2.034	A2734	0.0625	3	80
RXCJ0012.9-0853	00 12 54.7	-08 53 03	0.090±0.020	0.32±0.17	336	3.32	5.000 ^e	1.86					
RXCJ0013.6-1930	00 13 38.2	-19 30 08	0.306±0.035	0.48±0.11	313	2.04	4.699 ^e	6.09	2.355	A13	0.0949	1	4
RXCJ0014.3-3022	00 14 20.1	-30 22 33	0.250±0.047	0.23±0.15	122	1.65	11.184 ^e	4.96	19.331	A2744	0.3067	8	34
RXCJ0015.5-2346	00 15 31.8	-23 46 13	0.175±0.032	0.36±0.19	277	2.45	2.814 ^e	3.48	0.647	A14	0.0655	3	9
RXCJ0016.3-3121	00 16 19.8	-31 21 55	0.178±0.032	0.00±0.14	296	1.88	3.292 ^e	3.50	0.981	A2751	0.0805	20	1
RXCJ0017.5-3511	00 17 34.9	-35 11 09	0.166±0.033	0.28±0.17	354	1.31	3.686 ^e	3.22	1.304	A2755	0.0969	8	18
RXCJ0019.0-2026	00 19 03.9	-20 26 17	0.147±0.027	0.42±0.17	322	1.78	8.314 ^e	2.93	9.432	S26	0.2773	1	1
RXCJ0020.5-4913	00 20 34.1	-49 13 40	0.124±0.030	0.77±0.25	151	2.12	2.620 ^e	2.44	0.536	A2764	0.0711	3	19
RXCJ0020.7-2542	00 20 43.3	-25 42 53	0.289±0.035	0.48±0.12	281	2.26	6.360 ^e	5.81	4.921	A22	0.1410	3	3
RXCJ0024.0-1704	00 24 03.6	-17 04 32	0.088±0.019	0.63±0.24	314	2.00	4.956 ^e	1.75	2.680	A2768	0.1890	1	2
RXCJ0025.5-3302	00 25 32.2	-33 02 53	0.460±0.045	0.37±0.09	328	1.69	3.215 ^e	9.00	0.921	S41	0.0487	8	2
RXCJ0028.6-2338	00 28 39.5	-23 38 27	0.245±0.033	0.55±0.13	294	1.82	4.933 ^e	4.85	2.650	A42	0.1129	8	5
RXCJ0030.6-2410	00 30 37.6	-24 10 53	0.094±0.019	0.60±0.22	314	1.51	3.927 ^e	1.84	1.516	A47	0.1382	3	1
RXCJ0033.8-0750	00 33 51.6	-07 50 29	0.087±0.021	0.56±0.24	270	3.50	5.000 ^e	1.80		A56			
RXCJ0034.2-0204	00 34 13.9	-02 04 31	0.412±0.033	0.67±0.11	597	2.82	4.763 ^e	8.38	2.433	SH518	0.0822	11	1
RXCJ0035.6+0138	00 35 36.3	+01 38 20	0.105±0.022	0.75±0.23	291	2.66	5.000 ^e	2.13					
RXCJ0037.4-2831	00 37 27.0	-28 31 52	0.113±0.023	0.39±0.21	326	1.73	3.387 ^e	2.22	1.057	A2788	0.1050	3	20
RXCJ0041.8-0918	00 41 50.0	-09 18 12	3.554±0.114	0.63±0.03	328	3.58	6.200	74.00	9.810	A85	0.0556	12	116
RXCJ0042.1-2832	00 42 08.8	-28 32 12	0.498±0.049	0.28±0.07	325	1.49	6.768 ^e	9.82	5.726	A2811	0.1170	8	32
RXCJ0043.5-0443	00 43 34.6	-04 43 06	0.119±0.018	0.64±0.13	446	3.63	5.000 ^e	2.48					
RXCJ0048.6-2114	00 48 38.0	-21 14 50	0.217±0.032	0.09±0.13	339	1.52	2.759 ^e	4.20	0.614	A2824	0.0581	17	7
RXCJ0049.3-2931	00 49 23.8	-29 31 27	0.265±0.042	0.40±0.13	323	1.80	5.172 ^e	5.25	2.974	S84	0.1150	8	20
RXCJ0051.1-4833	00 51 11.2	-48 33 35	0.123±0.027	0.63±0.24	204	2.12	5.646 ^e	2.46	3.684	A2830	0.1873	1	2
RXCJ0051.3-2831	00 51 19.2	-28 31 10	0.127±0.023	0.40±0.16	324	1.63	3.750 ^e	2.49	1.359	A2839	0.1125	13	6
RXCJ0056.0-3732	00 56 01.0	-37 32 45	0.425±0.034	0.55±0.21	351	2.59	8.538 ^e	8.65	10.102		0.1663	2	11
RXCJ0056.3-0112	00 56 18.3	-01 12 53	1.644±0.087	0.74±0.06	321	3.10	5.100	33.70	2.855	A119	0.0444	17	23
RXCJ0058.4-1425	00 58 28.2	-14 25 39	0.108±0.018	0.17±0.15	492	1.87	3.105 ^e	2.12	0.840	A123	0.0957	5	2
RXCJ0102.7-2152	01 02 42.3	-21 52 46	0.970±0.065	0.33±0.06	268	1.48	3.800	18.90	2.574	A133	0.0562	8	9
RXCJ0104.5-2400	01 04 35.0	-24 00 00	0.119±0.021	0.64±0.19	335	1.61	4.672 ^e	2.34	2.322	A140	0.1520	8	12
RXCJ0105.5-2439	01 05 35.4	-24 39 33	0.196±0.031	0.32±0.12	326	1.61	8.018 ^e	3.88	8.635	A141	0.2300	8	1
RXCJ0106.8-0229	01 06 51.5	-02 29 18	0.152±0.032	0.91±0.23	423	4.10	6.386 ^e	3.21	4.972	A145	0.1909	5	1
RXCJ0107.8-3643	01 07 49.4	-36 43 44	0.180±0.024	0.82±0.16	378	1.94	4.642 ^e	3.57	2.285	A2871	0.1221	2	11
RXCJ0108.2+0210	01 08 12.8	+02 10 48	0.230±0.037	0.59±0.15	415	3.01	2.342 ^e	4.60	0.398	A147	0.0447	3	11
RXCJ0108.5-4021	01 08 33.2	-40 21 00	0.150±0.035	0.40±0.23	377	3.04	4.898 ^e	3.07	2.610	A2874	0.1408	13	6
RXCJ0108.8-1524	01 08 49.3	-15 24 30	0.358±0.035	0.29±0.08	446	1.69	3.149 ^e	7.00	0.872	A151	0.0537	8	37
RXCJ0108.9-1537	01 08 55.5	-15 37 42	0.189±0.029	0.46±0.09	437	1.69	3.954 ^e	3.72	1.541		0.0981	4,19	9
RXCJ0110.0-4555	01 10 00.7	-45 55 24	0.756±0.060	0.26±0.08	301	2.10	3.500	15.00	0.404	A2877	0.0250	8	109
RXCJ0113.9-3145	01 13 54.2	-31 45 07	0.080±0.017	0.58±0.24	333	2.40	1.000 ^e	1.21	0.018	S141	0.0184	8	18
RXCJ0114.7-2118	01 14 47.3	-21 18 02	0.082±0.018	0.56±0.24	346	1.49	5.000 ^e	1.61					
RXCJ0114.9+0024	01 14 57.5	+00 24 20	0.520±0.048	0.47±0.09	406	3.32	2.600	10.60	1.043	A168	0.0477	1	2
RXCJ0116.1-1555	01 16 11.8	-15 55 24	0.130±0.023	0.23±0.17	394	1.69	1.862 ^e	2.46	0.214	SCG 16	0.0448	1	2
RXCJ0118.1-2658	01 18 10.2	-26 58 18	0.193±0.027	0.54±0.14	366	1.47	7.987 ^e	3.81	8.554	A2895	0.2310	1	1
RXCJ0120.9-1351	01 20 57.9	-13 51 19	0.425±0.034	0.30±0.07	344	1.73	3.240 ^e	8.33	0.939	CID 10	0.0511	1	3
RXCJ0121.8-2022	01 21 48.1	-20 22 34	0.110±0.020	0.70±0.28	465	1.45	5.000 ^e	2.16		A2902			
RXCJ0122.2-2131	01 22 12.4	-21 31 04	0.097±0.020	0.05±0.17	494	1.39	5.000 ^e	1.90		A185			
RXCJ0122.9-1245	01 22 55.1	-12 45 50	0.096±0.018	0.87±0.25	391	1.68	3.598 ^e	1.88	1.229	A188	0.1230	3	2
RXCJ0125.4+0145	01 25 29.9	+01 45 46	0.425±0.034	0.77±0.15	413	3.08	1.446 ^e	8.03	0.107	NGC 533	0.0176	2	4
RXCJ0125.6-0125	01 25 38.0	-01 25 03	0.610±0.086	0.84±0.14	431	3.56	1.900	12.20	0.176	A194	0.0183	8	81
RXCJ0126.0-3758	01 26 04.6	-37 58 36	0.105±0.019	0.76±0.23	351	1.68	2.703 ^e	2.04	0.581	A2911	0.0810	4	31
RXCJ0126.7-1810	01 26 44.4	-18 10 20	0.103±0.025	0.32±0.21	328	1.62	5.000 ^e	2.03		A197			
RXCJ0127.2-1746	01 27 13.9	-17 46 17	0.109±0.021	0.28±0.19	351	1.52	4.358 ^e	2.14	1.960	A199	0.1459	1	2
RXCJ0131.7+0033	01 31 42.4	+00 33 43	0.088±0.017	0.26±0.18	432	2.92	2.535 ^e	1.77	0.490	A208	0.0798	3	?
RXCJ0131.8-1336	01 31 53.5	-13 36 27	0.277±0.029	0.33±0.10	453	2.27	8.513 ^e	5.59	9.982	A209	0.2060	3	2
RXCJ0137.2-0912	01 37 15.3	-09 12 10	0.425±0.034	0.68±0.08	444	2.75	2.672 ^e	8.50	0.564		0.0392	1	3
RXCJ0137.4-1259	01 37 29.2	-12 59 10	0.088±0.016	0.55±0.18	458	2.45	5.503 ^e	1.78	3.462	A222	0.2134	8	6
RXCJ0137.9-1248	01 37 56.4	-12 48 01	0.115±0.018	0.60±0.20	454	1.84	5.935 ^e	2.28	4.160	A223	0.2070	8	4
RXCJ0139.1-1915	01 39 10.1	-19 15 34	0.083±0.015	0.28±0.20	479	1.45	5.000 ^e	1.63					
RXCJ0139.9-0555	01 39 59.7	-05 55 23	0.084±0.018	0.43±0.20	441	2.85	5.000 ^e	1.71					

Table 3—Continued

Source (1)	RA (J2000) (2)	Decl (J2000) (3)	Count rate (4)	HR (5)	Time (6)	N_H (7)	T_x (8)	f_x (9)	L_x (10)	Identification (11)	Redshift (12)	Ref(z) (13)	N_g (14)
RXCJ0143.4-4614	01 43 29.8	-46 14 20	0.082±0.017	0.41±0.25	455	2.30	5.000 ^e	1.65		A2937			
RXCJ0144.6-2213	01 44 41.8	-22 13 43	0.097±0.015	0.25±0.13	494	1.18	6.991 ^e	1.90	6.196	A2938	0.2781	1	1
RXCJ0148.2-3155	01 48 14.8	-31 55 08	0.105±0.016	0.37±0.17	521	1.53	3.400	2.05		A2943			
RXCJ0148.3-0406	01 48 22.2	-04 06 13	0.104±0.024	0.25±0.19	255	2.59	5.000 ^e	2.10					
RXCJ0152.5-2853	01 52 32.8	-28 53 32	0.084±0.016	0.16±0.16	391	1.51	5.000 ^e	1.65					
RXCJ0152.7+0100	01 52 43.6	+01 00 58	0.151±0.022	0.42±0.13	407	2.84	7.309 ^e	3.09	6.900	A267 dc	0.2300	9	1
RXCJ0152.9-1345	01 52 59.8	-13 45 07	0.425±0.034	0.25±0.13	462	1.69	1.000 ^e	6.30	0.009	NGC 720	0.0057	15	1
RXCJ0153.5-0118	01 53 32.0	-01 18 44	0.123±0.030	0.54±0.17	433	2.66	7.025 ^e	2.50	6.277		0.2438	1	2
RXCJ0157.5-0549	01 57 30.5	-05 49 32	0.164±0.024	0.55±0.19	414	2.31	4.681 ^e	3.29	2.332	A281 dc	0.1285	2	2
RXCJ0158.4-0146	01 58 28.4	-01 46 51	0.116±0.020	0.48±0.17	406	2.55	4.948 ^e	2.34	2.672	A286	0.1632	1	1
RXCJ0201.7-0211	02 01 44.3	-02 11 58	0.209±0.024	0.52±0.11	406	2.57	7.327 ^e	4.25	6.941	A291	0.1965	9	1
RXCJ0202.3-4447	02 02 18.8	-44 47 37	0.124±0.020	0.31±0.18	465	2.70	2.359 ^e	2.46	0.405		0.0616	1	2
RXCJ0202.3-0107	02 02 20.6	-01 07 06	0.191±0.026	0.22±0.13	405	2.58	2.103 ^e	3.76	0.298	A295	0.0428	5	3
RXCJ0206.4-1453	02 06 29.9	-14 53 37	0.149±0.027	0.52±0.16	274	2.45	5.192 ^e	3.00	3.003	A305	0.1529	1	2
RXCJ0208.0-1537	02 08 00.2	-15 37 05	0.085±0.019	0.92±0.24	286	2.38	5.000 ^e	1.71					
RXCJ0211.4-4017	02 11 25.2	-40 17 09	0.166±0.019	0.54±0.14	583	1.43	3.859 ^e	3.24	1.457	A2984	0.1022	8	6
RXCJ0212.8-4707	02 12 53.9	-47 07 58	0.197±0.026	0.35±0.18	517	2.12	4.598 ^e	3.93	2.232	A2988	0.1150	25	?
RXCJ0213.9-0253	02 13 56.6	-02 53 53	0.101±0.022	0.46±0.20	350	2.16	5.000 ^e	2.02					
RXCJ0214.6-0433	02 14 41.1	-04 33 48	0.106±0.021	0.68±0.30	357	2.21	4.181 ^e	2.12	1.772	A329	0.1393	1	2
RXCJ0216.3-4816	02 16 19.1	-48 16 23	0.140±0.019	0.85±0.23	542	2.95	5.573 ^e	2.86	3.568	A2998	0.1709	1	1
RXCJ0216.7-4749	02 16 43.3	-47 49 31	0.180±0.030	0.89±0.28	523	2.95	2.809 ^e	3.63	0.644	S239	0.0640	23	1
RXCJ0218.3-3141	02 18 19.6	-31 41 34	0.099±0.016	0.28±0.14	486	1.87	5.000 ^e	1.96					
RXCJ0219.1-1724	02 19 08.3	-17 24 40	0.085±0.016	0.82±0.23	390	2.99	5.000 ^e	1.74					
RXCJ0220.9-3829	02 20 56.8	-38 29 02	0.425±0.034	0.74±0.17	558	1.85	10.965 ^e	8.48	18.532		0.2287	2	6
RXCJ0225.1-2928	02 25 10.2	-29 28 23	0.425±0.034	0.63±0.15	445	1.70	3.710 ^e	8.35	1.327		0.0607	1	2
RXCJ0225.8-4154	02 25 53.7	-41 54 19	0.258±0.029	0.29±0.10	460	2.14	8.693 ^e	5.19	10.503	A3017	0.2195	1	1
RXCJ0227.2-2851	02 27 12.6	-28 51 18	0.071±0.018	0.59±0.21	343	1.55	5.003 ^e	1.40	2.743	EDCC651	0.2138	2	?
RXCJ0229.3-3332	02 29 22.3	-33 32 13	0.198±0.026	0.34±0.12	471	2.07	3.352 ^e	3.92	1.029	APMCC269	0.0779	1	2
RXCJ0229.9-1316	02 29 56.4	-13 16 12	0.127±0.026	0.25±0.20	312	2.04	5.000 ^e	2.53					
RXCJ0230.8-3305	02 30 51.2	-33 05 49	0.166±0.026	0.71±0.24	456	1.96	3.116 ^e	3.27	0.848	A3027	0.0774	13	4
RXCJ0231.7-0451	02 31 47.3	-04 51 21	0.124±0.033	0.55±0.24	125	2.55	5.619 ^e	2.51	3.640	A362	0.1843	1	3
RXCJ0231.9+0114	02 31 57.5	+01 14 38	0.425±0.034	0.97±0.26	227	2.56	1.714 ^e	8.12	0.171		0.0221	1	2
RXCJ0232.2-4420	02 32 17.2	-44 20 43	0.425±0.034	0.14±0.09	369	2.61	13.183 ^e	8.66	28.933		0.2836	1	2
RXCJ0236.6-1923	02 36 39.6	-19 23 05	0.171±0.025	0.57±0.19	349	2.65	4.100	3.45	1.179	A367	0.0891	17	3
RXCJ0237.4-2630	02 37 29.0	-26 30 13	0.156±0.024	0.43±0.16	325	1.56	7.042 ^e	3.08	6.305	A368	0.2200	2	1
RXCJ0241.3-2839	02 41 20.9	-28 39 27	0.130±0.021	0.10±0.13	423	1.56	4.300	2.55	5.942	A3041	0.2323	1	3
RXCJ0244.1-2611	02 44 06.3	-26 11 07	0.152±0.027	0.79±0.25	286	1.74	4.726 ^e	3.00	2.389		0.1362	4,19	6
RXCJ0245.2-4627	02 45 12.6	-46 27 14	0.114±0.017	0.66±0.22	539	3.15	2.986 ^e	2.32	0.757	A3047	0.0868	1	1
RXCJ0248.0-0332	02 48 02.6	-03 32 09	0.229±0.042	0.49±0.16	224	4.12	7.521 ^e	4.85	7.396	A383	0.1899	1	1
RXCJ0248.2-0216	02 48 16.3	-02 16 44	0.220±0.033	0.66±0.22	117	3.65	8.748 ^e	4.60	10.743	A384	0.2360	2	?
RXCJ0249.6-3111	02 49 36.9	-31 11 19	0.469±0.040	1.31±0.27	419	1.80	1.837 ^e	8.89	0.206	S301	0.0232	8	34
RXCJ0251.4-2456	02 51 28.8	-24 56 58	0.144±0.023	0.04±0.12	365	1.90	4.500	2.85	1.511	A389	0.1111	8	6
RXCJ0251.7-4109	02 51 42.3	-41 09 00	0.102±0.018	0.00±0.17	496	1.86	5.000 ^e	2.02					
RXCJ0252.8-0116	02 52 50.1	-01 16 28	0.425±0.034	1.34±0.23	135	5.25	1.833 ^e	8.84	0.205	NGC 1132	0.0232	10	1
RXCJ0258.2-2105	02 58 15.0	-21 05 29	0.114±0.023	0.57±0.21	287	1.92	3.859 ^e	2.25	1.458	A3073	0.1226	1	1
RXCJ0303.2-2735	03 03 14.8	-27 35 59	0.122±0.028	0.25±0.20	266	1.55	5.000 ^e	2.40		A3082			
RXCJ0303.3+0155	03 03 21.3	+01 55 35	0.219±0.033	0.83±0.15	222	7.82	6.421 ^e	5.08	5.062	A409	0.1530	9	1
RXCJ0304.0-3656	03 04 06.0	-36 56 32	0.151±0.023	0.76±0.23	384	1.95	6.958 ^e	3.01	6.120	A3084	0.2192	2	?
RXCJ0307.0-2840	03 07 04.0	-28 40 15	0.197±0.034	0.38±0.15	237	1.36	8.674 ^e	3.88	10.434	A3088	0.2534	7	?
RXCJ0311.4-2654	03 11 25.3	-26 54 00	0.154±0.078	0.52±0.22	210	1.56	2.722 ^e	2.98	0.593	A3094/EDCC736 dc	0.0677	3	67
RXCJ0313.6-3817	03 13 38.0	-38 17 55	0.119±0.023	0.20±0.22	321	2.03	2.905 ^e	2.34	0.704	A3098	0.0833	3	6
RXCJ0314.3-4525	03 14 19.6	-45 25 24	0.401±0.038	0.45±0.10	313	3.57	4.252 ^e	8.31	1.845	A3104	0.0718	2	4
RXCJ0317.7-4848	03 17 46.4	-48 48 42	0.097±0.016	0.56±0.23	487	2.06	5.000 ^e	1.93		A3113			
RXCJ0317.9-4414	03 17 58.2	-44 14 16	1.447±0.056	0.30±0.04	481	2.53	4.100	29.10	7.130	A3112	0.0754	1	2